Effects of temperature variations on the modal properties of masonry structures: An experimental-based numerical modelling approach

D. Pellegrini [a],[*], A. Barontini [b], M. Girardi [a], P.B. Lourenço [b], M.G. Masciotta [c],[a], N. Mendes [b], C. Padovani [a], L.F. Ramos [b]

[a] Institute of Information Science and Technologies "A. Faedo", ISTI–CNR, Pisa, Italy
[b] ISISE, Department of Civil Engineering, University of Minho, Guimarães, Portugal
[c] Department of Engineering and Geology, University "G. D'Annunzio" of Chieti-Pescara, Pescara, Italy

ABSTRACT

Long–term ambient vibration monitoring campaigns show that environmental parameters (such as temperature, humidity, wind speed and direction) can influence the structures' static and dynamic behaviour. In particular, thermal variations can affect the modal characteristics of ancient masonry constructions. This work presents a procedure combining experimental and numerical steps to monitor, assess and model the dynamic behaviour of masonry structures subjected to thermal loads. The procedure is tested and validated through two numerical examples and the simulation of a full-scale masonry structure, the Mogadouro clock tower in Portugal, monitored with accelerometers and temperature and humidity sensors.

1. Introduction

The influence of thermal variations on the mechanical behaviour of materials with low tensile strength is a well-known phenomenon that has been observed in many different cases. Practical examples range from masonry bridges and monuments, in which temperature changes typically induce displacement and stress variations [1] and modify the crack distribution [2,3], to stone arches, whose dynamic properties closely depend on daily and yearly thermal fluctuations [4]. In instances such as the thermo-mechanical process undergone by the refractory structures used in the iron and steel industry [5], the thermal variation is so high that the dependence of the material characteristics on temperature cannot be disregarded [6].

Several Structural Health Monitoring (SHM) campaigns have shown that thermal variations influence not only the static behaviour of masonry structures but also their dynamic features. For instance, slender masonry structures, like towers and bell towers, generally exhibit frequency upshifts for increasing temperature, unlike concrete and steel structures, which usually show an opposite trend. Such behaviour can be attributed to the stiffness increment associated with the micro-cracks closure and the reduction in moisture content induced by higher temperatures. An inverse trend can be observed for low temperatures,

typically around 0 °C, because of the formation of ice in the micropores and voids of the masonry with temporary increase of the material stiffness and natural frequencies. Although nonlinear frequency-temperature relationships can emerge in case of complicated temperature-driven mechanisms [7], many studies have shown that the typical correlation between frequencies and temperature is bilinear, with a vertex close to the freezing point [8–13].

Thermal variations in masonry structures may be responsible for other phenomena at a local level, such as growing thrusts in arches, increase of tilting movements or loss of tension in metallic tie-rods, thus resulting in global softening effects and frequency downshifts [12,14]. These phenomena typically affect high-frequency mode shapes; nonetheless, negative frequency-temperature correlations for lower modes have been observed in several cases, such as the cathedral of Milan (Italy) [15], the Consoli Palace in Gubbio (Italy) [7] and the Basilica of Santa Maria di Collemaggio in L'Aquila (Italy) [16]. While in the first two cases the decrease in frequencies as the temperature increases was attributed to the presence of tie rods across the structure, in the last case the inverse frequency-temperature correlation was attributed to the global stiffness reduction induced by the cross-laminated timber roof expansion at higher temperatures. As far as laboratory tests on masonry structures are concerned, in [17] a circular masonry arch subjected to
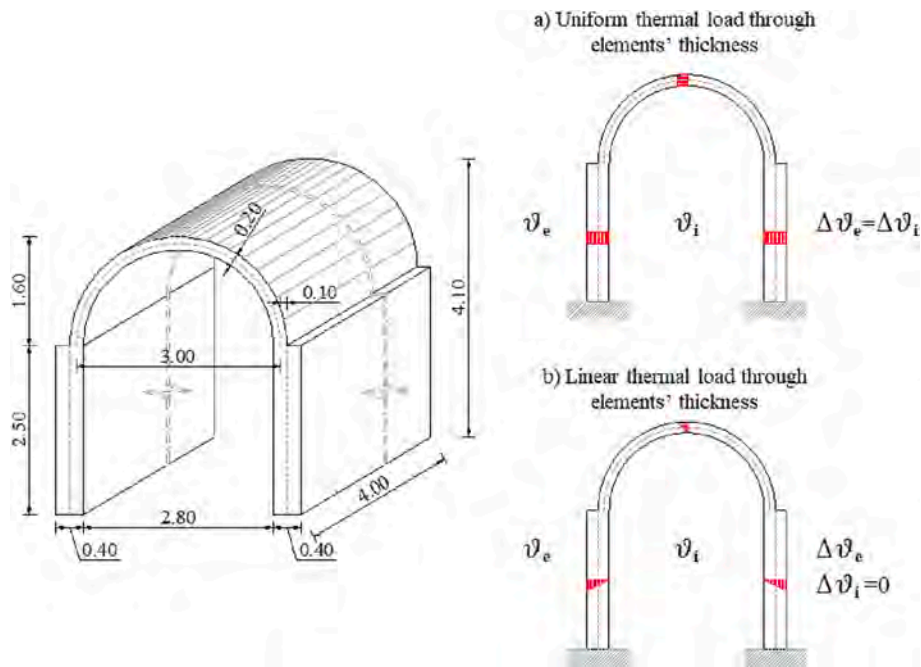
Fig. 1. Geometry of the structure (dimensions in meters) with through-thickness uniform (*case a*) and linear (*case b*) temperature variation distributions.
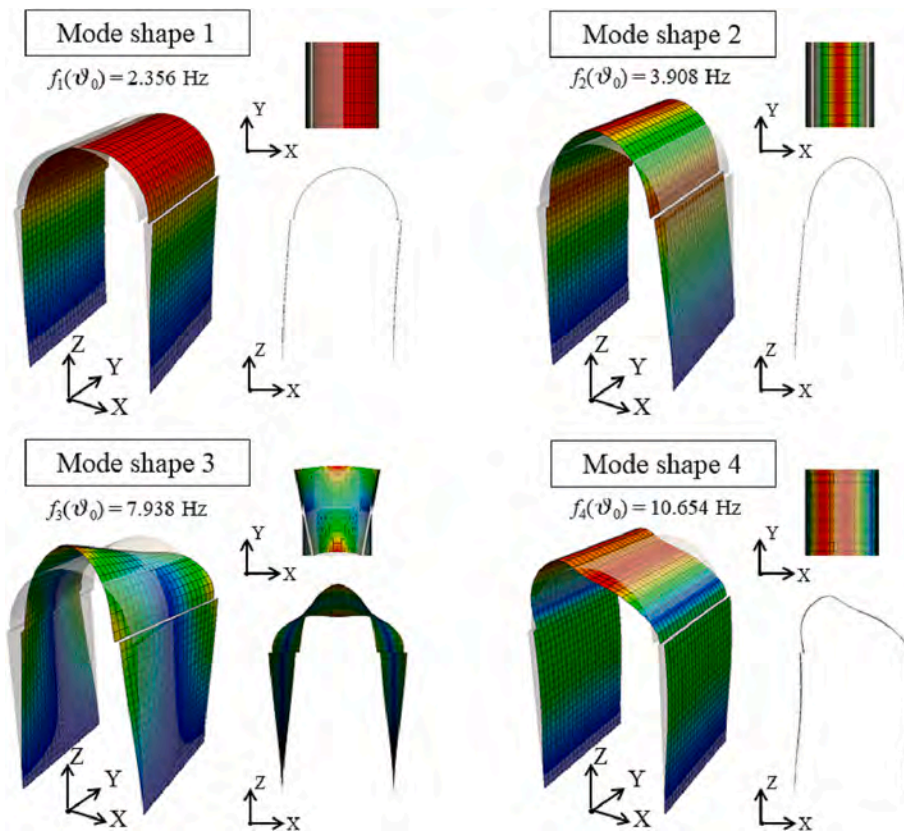

Fig. 2. First four frequencies and mode shapes of the unconstrained barrel vault at reference temperature ϑ_0.

thermal and moisture content variations has been monitored to assess their influence on the natural frequencies and mode shapes of the arch.

In addition, it must be stressed that the behaviour of historical masonry structures can also be governed by the interaction of different macro-elements, i.e. portions of masonry macroscopically homogeneous and bounded by lines of weak connection. This means that the thermally induced relative displacements of such elements can modify the connections between masonry portions and significantly affect the modal properties, causing unexpected trends or even abrupt shifts in the natural frequencies. The case study of the Ghirlandina tower in Modena (Italy) represents a relevant example in this regard, as the lowering of temperature values led the tower to move towards the cathedral, with
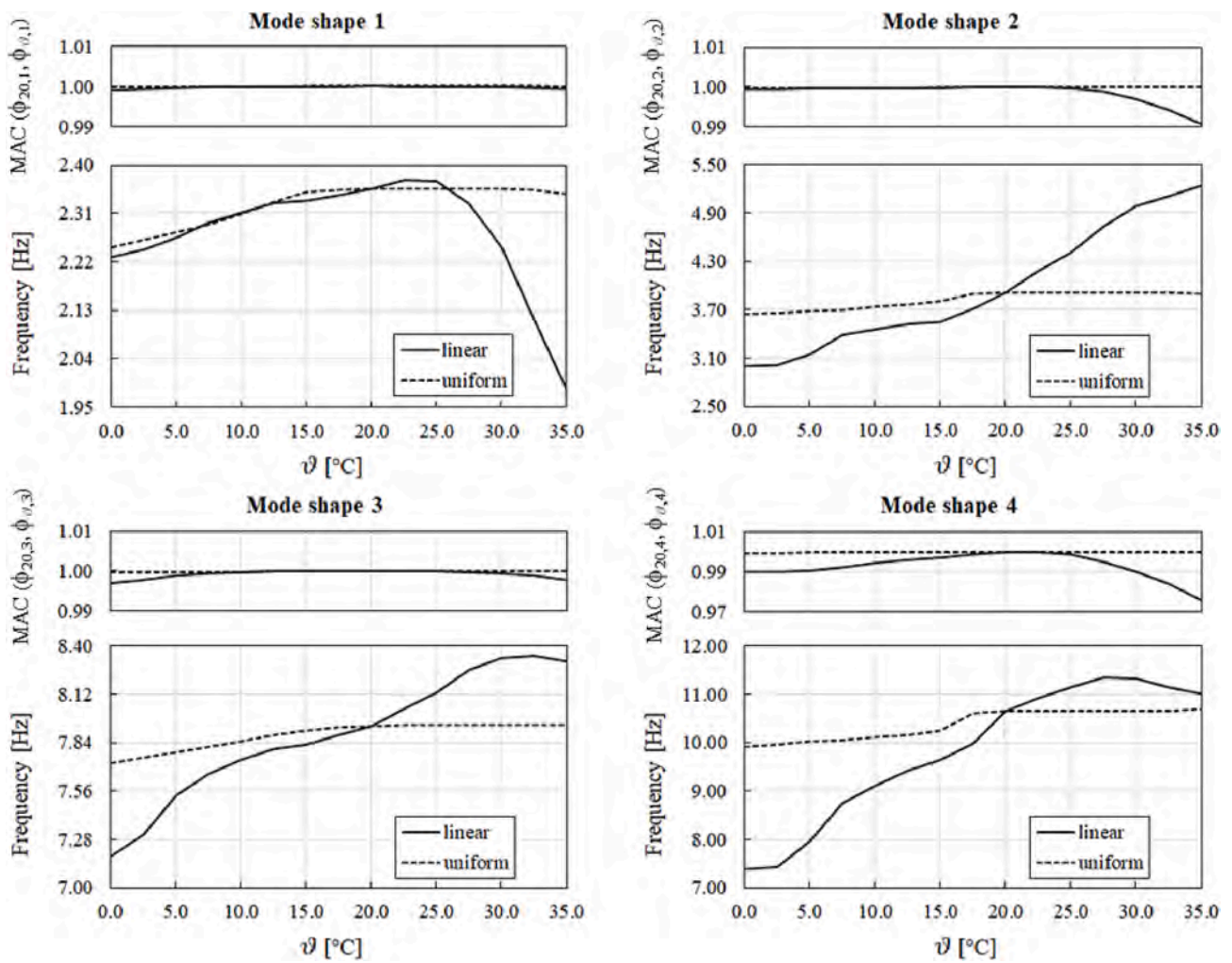
Fig. 3. Evolution of the frequencies and MAC values of the system mode shapes with varying temperature in case of uniform (*case a* - dashed black line) and linear (*case b* - solid black line) thermal distribution within the walls. Note the different vertical scales used.
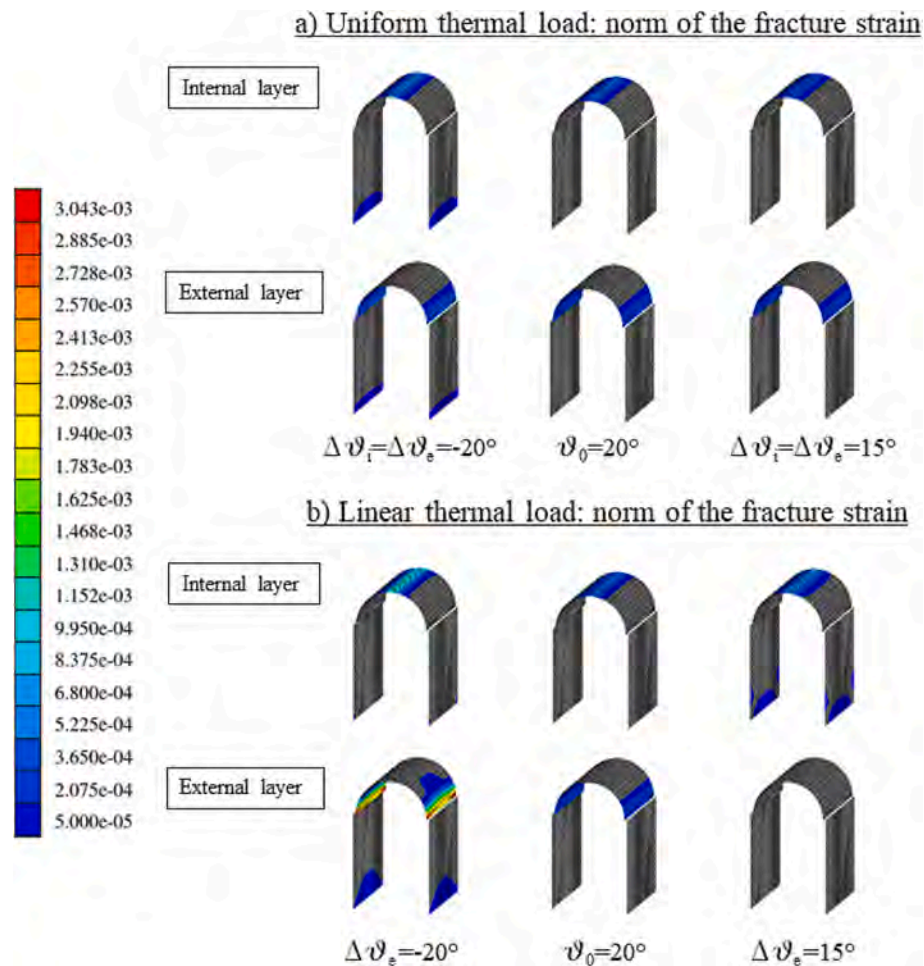
Fig. 4. Crack pattern in the vault under uniform (top) and linear (bottom) thermal load distributions in the configurations corresponding to the reference temperature ϑ_0 and to the lower and upper bounds of the temperature variation range $[\vartheta_1, \vartheta_2]$. (For interpretation of the references to colour in this figure legend, the reader is referred to the web version of this article).

Table 1

Case a: natural frequencies of the unconstrained vault at ϑ_0 (f_0), ϑ_1 (f_1) and ϑ_2 (f_2); relative frequency variation $\Delta f_1 = (f_1 - f_0)/f_0$ and $\Delta f_2 = (f_2 - f_0)/f_0$; MAC values between the mode shapes $\phi_{0,i}$ (i = 1…4) and the corresponding ones at ϑ_1 (MAC$_1$) and ϑ_2 (MAC$_2$).

Mode shape	f_0 [Hz]	f_1 [Hz]	Δf_1 [%]	MAC$_1$ [-]	f_2 [Hz]	Δf_2 [%]	MAC$_2$ [-]
ϕ_1	2.356	2.248	−4.57	0.999	2.346	−0.40	1.000
ϕ_2	3.908	3.646	−6.70	0.999	3.902	−0.15	1.000
ϕ_3	7.938	7.722	−2.71	0.999	7.944	0.08	1.000
ϕ_4	10.654	9.915	−6.93	0.999	10.706	0.49	1.000

consequent alterations of its boundary conditions as well as of its intrinsic modal features [18].

From a numerical point of view, two viable strategies have been developed for simulating, predicting and possibly removing – from the collected field data – the thermal effects in masonry materials, namely data-driven approaches or finite element simulations. The former has been the object of extensive investigations, giving rise to several new statistical ways to address the problem [19–29]. However, these approaches are often unable to explain the evolution of natural frequencies over time by resorting to a unique independent variable (the temperature), as more predictors may influence at the same time the dynamic behaviour of masonry artefacts [30]. Conversely, studies based on Finite Element (FE) analyses aimed at replicating the thermal effects on masonry structures' behaviour own a great potential and are relatively

scarce. Noteworthy examples are the uncoupled thermo-mechanical simulation used in [31] to explain the presence of a dominant crack in the South wall of Torre Astesiano (Italy), and the FE model developed in [32] to analyse the structural condition of the Basilica of San Vitale in Ravenna (Italy) taking into account the effects of seasonal thermal variations.

An in-depth investigation on the numerical modelling of the static behaviour of masonry solids subjected to thermal loads was addressed in [33], where the constitutive equation of masonry-like materials [6,34] is generalized to the non-isothermal case to consider thermal dilatations due to temperature variations. The generalized equation has been implemented in NOSA-ITACA (www.nosaitaca.it/software/), a FE code for the structural analysis of masonry constructions in non-isothermal conditions. This tool has been exploited to analyse the influence of the

Table 2

Case b: natural frequencies of the unconstrained vault at ϑ_0 (f_0), ϑ_1 (f_1) and ϑ_2 (f_2); relative frequency variation $\Delta f_1 = (f_1 - f_0)/f_0$ and $\Delta f_2 = (f_2 - f_0)/f_0$; MAC values between the mode shapes $\phi_{0,i}$ (i = 1…4) and the corresponding ones at ϑ_1 (MAC$_1$) and ϑ_2 (MAC$_2$).

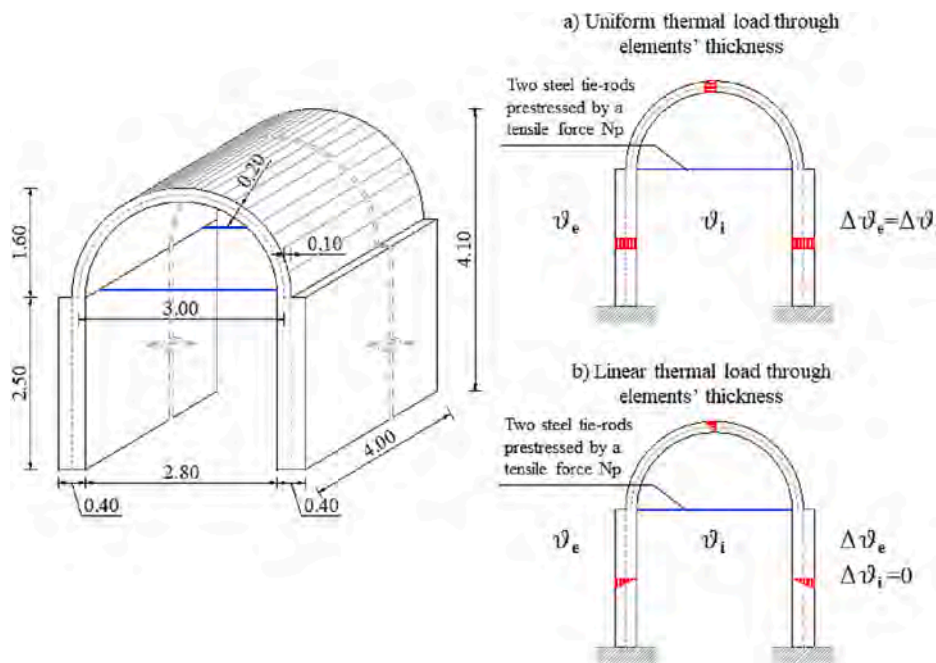| Mode shape	f_0 [Hz]	f_1 [Hz]	Δf_1 [%]	MAC$_1$ [-]	f_2 [Hz]	Δf_2 [%]	MAC$_2$ [-]
ϕ_1	2.356	2.230	−5.35	0.999	1.984	−15.76	0.999
ϕ_2	3.908	2.993	−23.42	0.999	5.246	34.23	0.990
ϕ_3	7.938	7.181	−9.54	0.996	8.311	4.71	0.997
ϕ_4	10.654	7.381	−30.72	0.989	11.006	3.31	0.976

Fig. 5. Structure's scheme (dimensions in meters).

Table 3
Mechanical properties of the constituent materials of the vault reinforced with tie rods.

	Masonry	Steel
Young's modulus E [Pa]	$1.74 \bullet 10^9$	$2.1 \bullet 10^{11}$
Poisson's ratio ν	0.2	0.3
Mass density ρ [kg/m^3]	2100	7850
Thermal expansion coefficient α [°C^{-1}]	10^{-5}	$1.2 \bullet 10^{-5}$
Tensile strength σ_t [Pa]	10^5	–
Compressive strength σ_c [Pa]	Infinite	–

thermal variations on the dynamic characteristics of masonry constructions in [35], which describes a numerical procedure for considering the effects of thermal stresses on both natural frequencies and mode shapes. The procedure has been recently applied to two numerical case studies consisting of a circular arch and a segmental arch masonry bridge [36].

The present work originates from the necessity to provide a procedure combining both experimental and numerical stages in order to monitor, assess and model the dynamic behaviour of masonry structures subjected to thermal loads. To this end, the paper aims to present a method that allows taking into account, from a numerical point of view, the influence of environmental parameters on the variation of the dynamic characteristics of a structure. The procedure, grounded on the NOSA-ITACA code, is tested and validated through two numerical examples featuring analogous geometry but different stiffening elements, as well as through the simulation of a full-scale masonry structure, the Mogadouro clock tower in Portugal, monitored with accelerometers, and temperature and humidity sensors.

The paper is organised as follows. Section 2 describes the procedure put into practice for reproducing and evaluating the dynamic behaviour of masonry structures subjected to thermal loads. Section 3 presents a first numerical validation of the procedure by resorting to the numerical case study of a barrel vault on lateral walls, with and without tie-rod constraints. Section 4 analyses and discusses the effects of thermal changes on the dynamic behaviour of a real benchmark masonry tower. Finally, Section 5 summarises the main conclusions of this work.

2. Procedure's outline: Experimental and numerical analysis

The modal properties (i.e. frequencies, mode shapes and damping ratios) of old masonry constructions can be affected by environmental parameters (such as temperature, humidity, wind speed and direction, etc.) in different ways depending on various factors: structural typology [15,23,37,38], constituent materials and the relative mechanical characteristics [9,39], indoor and outdoor temperature distribution [40], and existence of stiffening structural elements [7,15]. Among the various environmental parameters listed above, temperature appears to be the one that most affects the behaviour of masonry structures.

In order to simulate the global dynamic behaviour of a monitored structure, considering the influence of thermal loads, it is necessary to define a proper procedure encompassing both experimental and numerical phases as summarized in the following steps:

a. To execute a survey with a preliminary ambient vibration test (AVT) to estimate the structure's modal properties (reference dynamic properties) and detect the presence of possible cracks;
b. To measure the internal and external structure's temperature during the preliminary AVT (reference temperature ϑ_0);
c. To conduct an experimental long-term monitoring campaign, comprising modal tracking, and continuous temperature measurements;
d. To build and calibrate the FE model of the structure via a nonlinear model updating technique to estimate the constituent materials' mechanical properties at the reference temperature ϑ_0;
e. To calculate the numerical frequencies and mode shapes of the structure for distinct temperature values detected during the experimental campaign.

The first three steps are related to the experimental structural health monitoring; whereas steps d. and e. are related to the numerical counterpart simulations, hence they can be achieved by means of a FE code able to model the nonlinear behaviour of the constituent materials and taking into account the effects of thermal loads on the structure's dynamic behaviour.

In the present work, all the numerical simulations are performed using NOSA-ITACA, a code developed by ISTI-CNR for the calibration
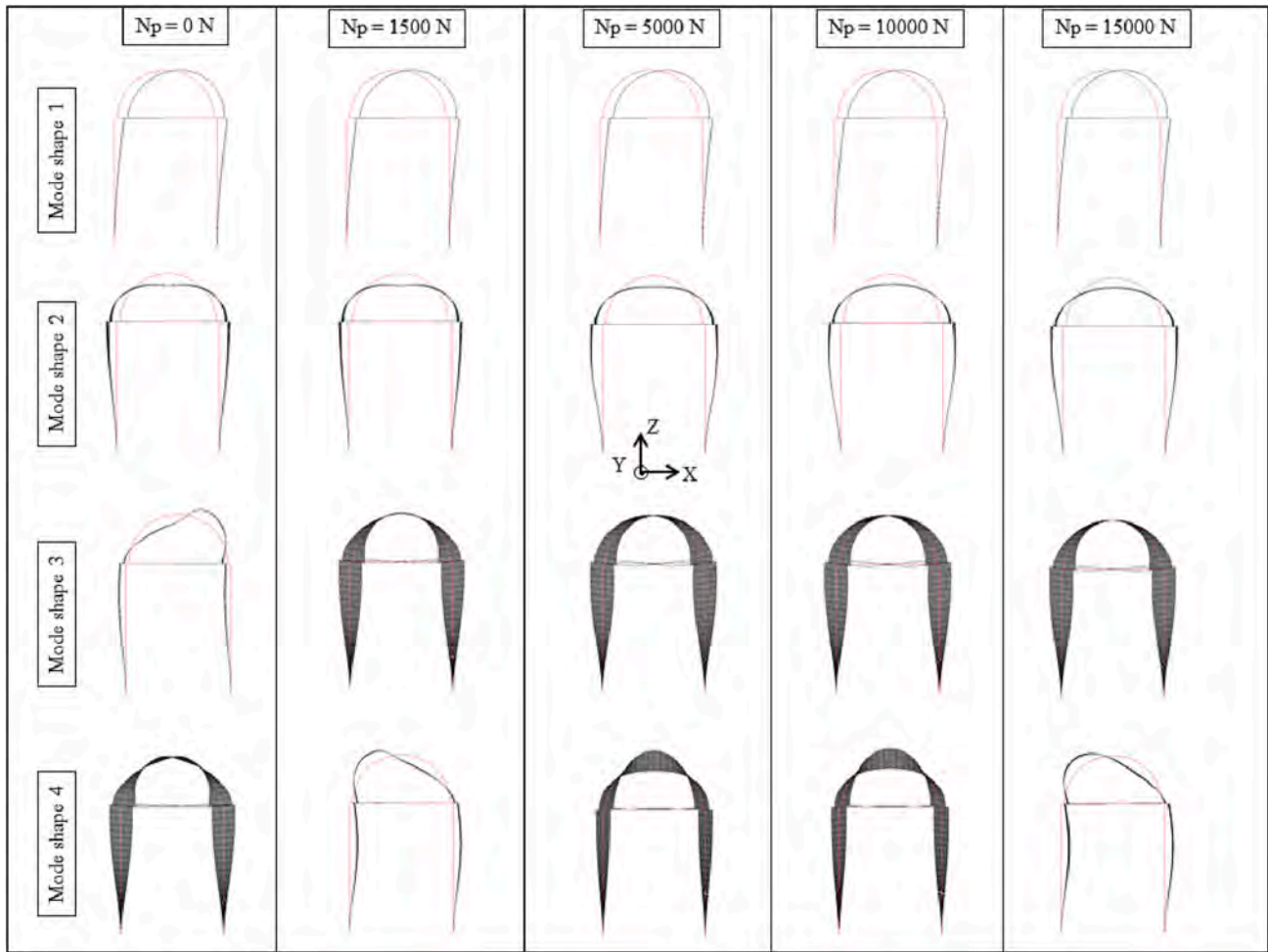
Fig. 6. Mode shapes of the vault, at the reference temperature, for varying values of preload force in the tie-rods.

and analysis of masonry structures subjected to thermal loads. Here, masonry is modelled as an isotropic homogeneous nonlinear elastic material with zero or low tensile strength σ_t and infinite or bounded compressive strength σ_c [6,35].

Using NOSA-ITACA, the natural frequencies and mode shapes of a masonry structure can be estimated, considering the crack distribution due to external loads, through a linear perturbation analysis. This numerical procedure, proposed in [35,41,42], consists of two steps. In the first step, the equilibrium problem of the structure discretized into finite elements and subjected to assigned loads and boundary conditions is solved through a Newton-Raphson iteration scheme, obtaining its displacements, stress and strain fields. In the second step, the tangent stiffness matrix, $\boldsymbol{K}^T$, is calculated by using the derivative of the stress with respect to the strain [6] obtained in the previous step, and the following generalized eigenvalue problem is solved using matrix $\boldsymbol{K}^T$ in place of the elastic stiffness matrix

$$\boldsymbol{K}^T \mathbf{v} = \omega^2 \boldsymbol{M} \mathbf{v} \tag{1}$$

where $\mathbf{v} \in \mathbb{R}^n$ is the vector of the structure's degrees of freedom and the integer n is the system's total number of degrees of freedom. The tangent stiffness matrix $\boldsymbol{K}^T \in \mathbb{R}^{n \times n}$ and the mass matrix $\boldsymbol{M} \in \mathbb{R}^{n \times n}$, symmetric and positive-definite, are obtained by assembling the elemental matrices and taking into account the constraints assigned to the displacements of the structure. Solving Eq. (1) provides the natural frequencies $f_i = \omega_i/2\pi$ and mode shapes $\mathbf{v}^{(i)}$ of the cracked structure [42]. Thus, the procedure allows to consider the effects of the stress field and cracks distribution within the structure on its natural frequencies and mode shapes.

The automated nonlinear model updating procedure proposed in [43] allows matching the numerical and experimental frequencies and mode shapes, as well as calibrating the model's free parameters, by coupling linear perturbation and modal analysis as described above.

The nonlinear model updating problem can be formulated as an optimization problem by assuming that the tangent stiffness and mass matrices are functions of the parameter vector $\mathbf{x}$, containing the Young's moduli, tensile strengths and density masses of the constituent materials. The goal is to determine the optimal value of $\mathbf{x}$ belonging to the p-dimensional box $\Omega = [a_1, b_1] \times \dots \times [a_p, b_p]$, which minimizes the following objective function $\Phi(\mathbf{x})$

$$\Phi(\mathbf{x}) = \sum_{i=1}^q w_i^2 \left[f_{i,\exp} - f_i(\mathbf{x}) \right]^2 \tag{2}$$

involving the vector $\mathbf{f_{exp}} \in \mathbb{R}^q$ of the experimental frequencies to match and the vector $\mathbf{f}(\mathbf{x}) \in \mathbb{R}^q$ of the numerical frequencies evaluated by solving Eq. (1), depending on the vector $\mathbf{x}$ of the p model's unknown parameters (with $p \leq q$), with w_i suitable weights. Function Φ is nonlinear as the frequencies $f_i(\mathbf{x})$ depend nonlinearly on $\mathbf{x}$, as in the classical case of linear elastic materials addressed in the literature [7,22,30,44–47]. Another source of nonlinearity of $\Phi(\mathbf{x})$ is here the dependence of $\boldsymbol{K}^T(\mathbf{x})$, and then of $\mathbf{f}(\mathbf{x})$, on the solution of the equilibrium problem dealt with in the first step. Function $\Phi(\mathbf{x})$ is not convex and the uniqueness of the minimum point cannot be assumed.

The method implemented in NOSA-ITACA to find the optimal value of $\mathbf{x}$ is based on an adaptive global polynomial interpolation of the objective function, which guarantees good global convergence
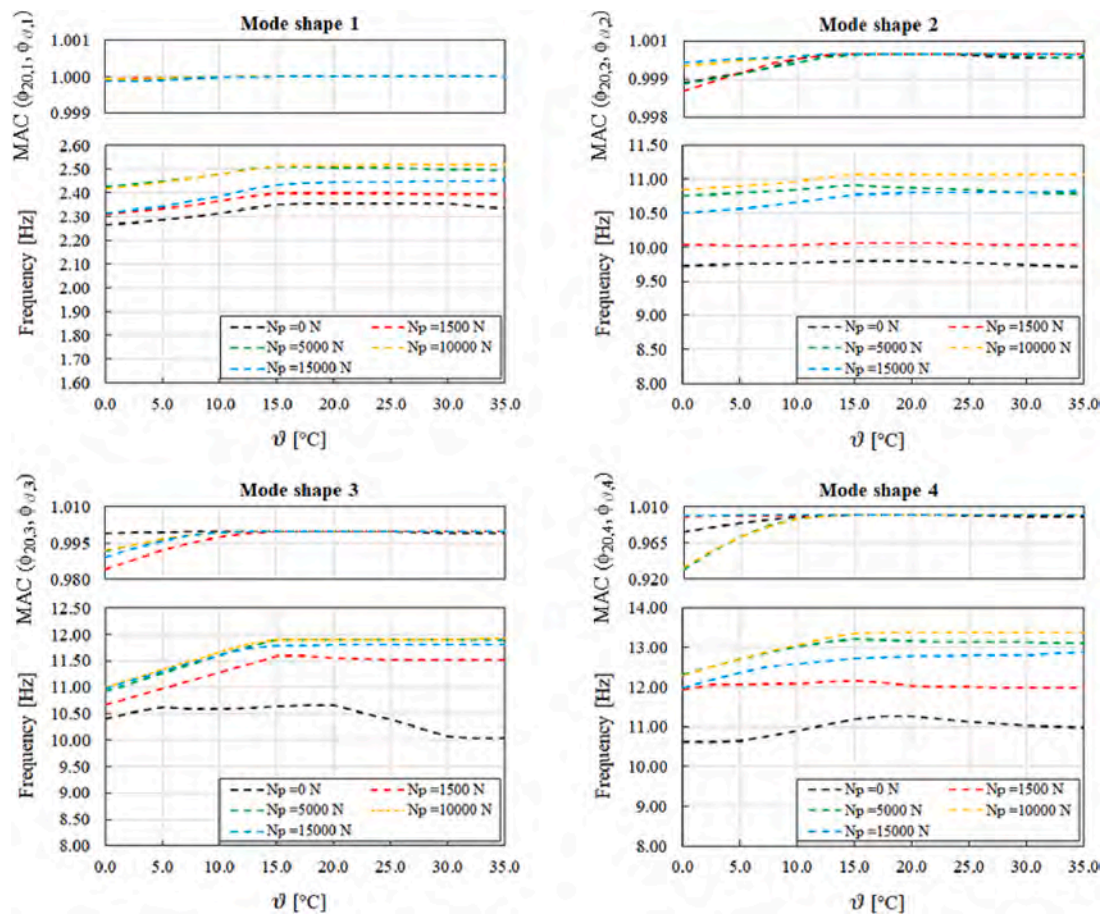
Fig. 7. Evolution of the frequencies and MAC values of the reinforced vault mode shapes with varying the temperature for different values of Np in case of uniform thermal load applied to the structure. Note the different vertical scales used. (For interpretation of the references to colour in this figure legend, the reader is referred to the web version of this article).

properties avoiding the convergence to local minima [43]. The main building block of this approach is the approximation of multivariate functions through Chebsyhev interpolation combined with adaptive cross approximation techniques. The proposed method allows to calculate a surrogate function $\Phi_k(\mathbf{x})$, which approximates the objective function $\Phi(\mathbf{x})$ on the whole domain Ω and is cheaper to calculate than $\Phi(\mathbf{x})$ and compute its global minimum.

3. Numerical examples

This section aims to demonstrate the ability of the numerical algorithms implemented to capture the dynamic properties of a masonry structure as a function of the temperature, under varying boundary conditions. For this purpose, two trial examples are considered hereafter, each featuring as a case study a masonry barrel vault on lateral walls subjected to a given thermal load history. The difference between the structures lies in the lack or presence of constraining steel tie rods.

3.1. A barrel vault on lateral walls

The first example is the barrel vault on lateral walls sketched in Fig. 1. The structure, fully clamped at the base of the walls, consists of a 4.0 m long vault with a thickness of 0.20 m, a mean radius of 1.5 m and a span of 3.0 m, resting on two lateral walls of 2.5 m height and 0.4 m thickness. The structure is discretized into 1280 thick curved shell elements, element no. 10 of the NOSA-ITACA library [48], resulting into a final model with 1407 nodes and 8442 degrees of freedom.

The structure is subjected to its self-weight and uniform (*case a*) or

linear (*case b*) temperature variations through the elements' thickness.

All the analyses are performed assuming that the vault and lateral walls are made of a masonry-like material with Young's modulus $E = 1.74 \bullet 10^9$ Pa, Poisson's ratio $\nu = 0.2$, density $\rho = 2100$ kg/m^3, tensile strength $\sigma_t = 10^5$ Pa, infinite compressive strength and linear thermal expansion coefficient $\alpha = 10^{-5}$ (°C)$^{-1}$. The mechanical properties of the masonry are assumed temperature-independent. The reference temperature ϑ_0 is set equal to 20 °C; ϑ is assumed varying in the interval $[\vartheta_1, \vartheta_2]$ with $\vartheta_1 = 0$ °C and $\vartheta_2 = 35$ °C, respectively. The thermal loads are applied incrementally. Denoting by ϑ_i and ϑ_e, respectively, the internal and external temperature values in the structure, it follows that for *case a*, the thermal variation increments equal each other, i.e., $\Delta\vartheta_e = \Delta\vartheta_i = \Delta\vartheta = \vartheta\text{-}\vartheta_0$; whereas for *case b*, the through-thickness temperature variation is not uniform, with $\Delta\vartheta_e = \Delta\vartheta = \vartheta\text{-}\vartheta_0$ and $\Delta\vartheta_i$ equal to zero. In both cases, $\Delta\vartheta$ ranges from -20 °C to 15 °C.

For each temperature increment, the equilibrium problem is solved and the natural frequencies $f_i(\vartheta)$ and mode shapes $\phi_i(\vartheta)$ (for i = 1,…,4) of the structure are calculated via the linear perturbation analysis implemented in NOSA-ITACA, and the MAC values [49] between the current mode shapes and those corresponding to the reference temperature ϑ_0 are estimated.

Fig. 2 summarizes the first four frequencies and mode shapes of the barrel vault without tie rods at the reference temperature ϑ_0. The first three mode shapes can be denoted as global modes as they involve the entire system (vault and walls). They correspond to a bending mode along the X direction (mode 1), a vertical bending mode along the Z-axis (mode 2) and a torsional mode shape symmetrical with respect to the ZY plane of the vault (mode 3). The fourth mode shape (mode 4) mainly
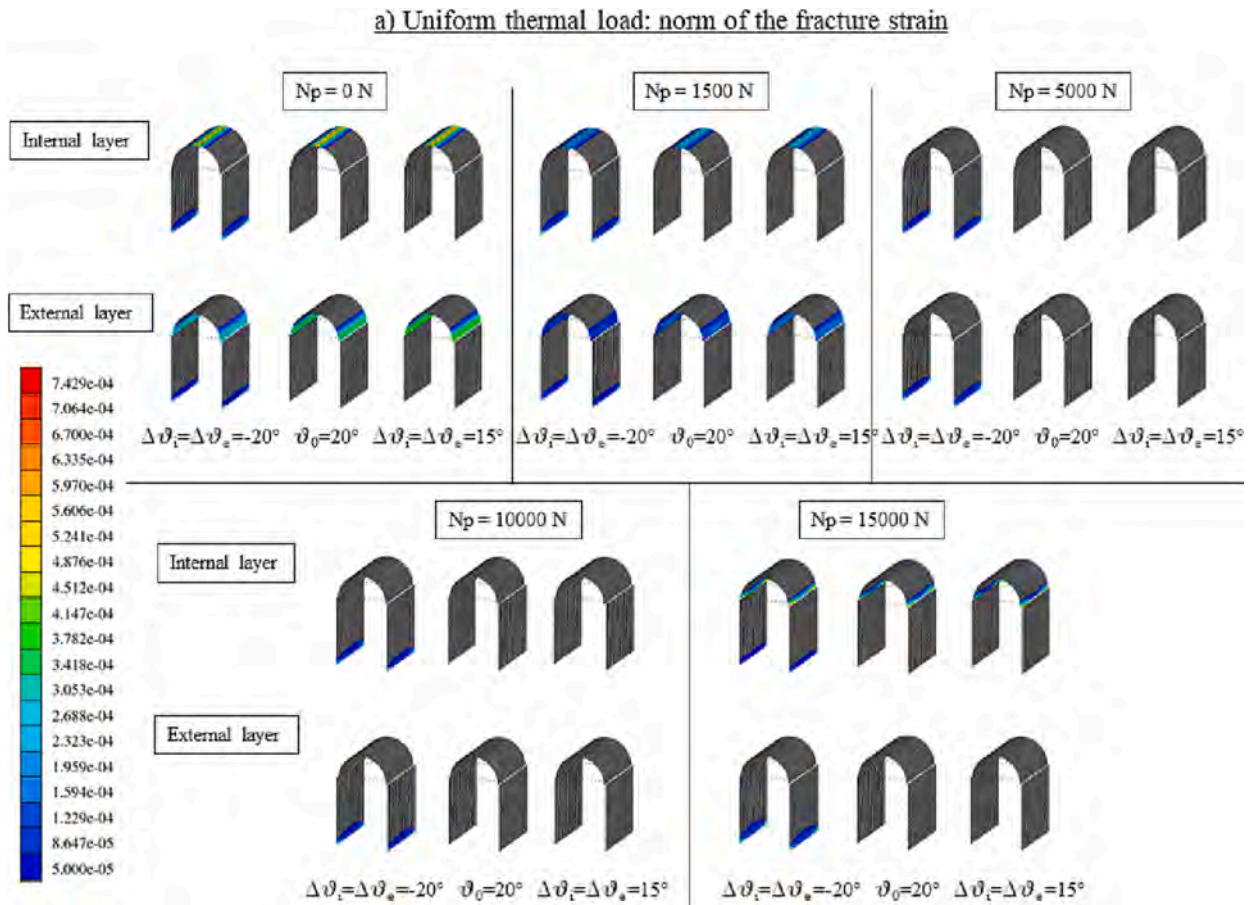
Fig. 8. Crack pattern in the vault for different values of Np under uniform thermal load distributions in the configurations corresponding to the reference temperature ϑ_0 and to the lower and upper bounds of the temperature variation range $[\vartheta_1, \vartheta_2]$. (For interpretation of the references to colour in this figure legend, the reader is referred to the web version of this article).

concerns the vaulted part and recalls the first asymmetrical mode shape typical of arched structures [50]. It is worth noting that the frequencies calculated via linear perturbation analysis differ from those obtained in a standard modal analysis because of the microfractures – at the intrados of the keystone section of the vault and at the extrados of the relative support sections (see also Fig. 4, temperature ϑ_0) – resulting from the application of the structure's self-weight. Indeed, masonry buildings may exhibit microcracks even for permanent loads, hence their intrinsic dynamic properties will differ depending on the presence of cracked regions [51].

Fig. 3 shows, for each mode shape and for each temperature value ϑ, the variation of frequencies and MAC values with respect to the modes estimated at the reference temperature ϑ_0 in case of uniform thermal distribution (*case a* - dashed black line) and through-thickness linear thermal distribution (*case b* - solid black line). The figure also shows the frequencies as a function of temperature (down) for *case a* (dashed black line) and *case b* (solid black line).

Fig. 4 shows the norm of the fracture strain tensor for both uniform (top) and linear (bottom) thermal loads at the intrados and extrados of the structure. In this regard, it is interesting to highlight the inverse correlation between fracture strain and temperature values, which corroborates the typical behaviour observed in the literature for masonry structures exposed to increasing temperature variations.

Tables 1 and 2 report, for both cases, the frequencies calculated at the bounds of the temperature variation range, as well as the relative frequency variation against the reference temperature scenario and the MAC values calculated, considering all degrees of freedom, between the mode shapes at ϑ_1 (or ϑ_2) and the corresponding ones at ϑ_0.

The analysis of the previous figures and tables demonstrates that in the case of uniform thermal load, for temperatures greater than 20 °C (ϑ_0), the vault undergoes no significant variation in terms of frequencies and mode shapes (0.40% for the fourth frequency). This outcome can be explained by observing the crack pattern reported in Fig. 4 (top plots), showing that the distribution of the cracks remains substantially unchanged and localized in the same areas as the temperature exceeds the initial reference value. Conversely, when the temperature decreases, the frequencies decrease likewise because of the development of additional cracks at the base of the lateral walls and the growth of fracture areas at the vault's keystone and springing sections.

In the case of linear thermal load, the system's dynamic characteristics differ substantially over the temperature interval. The first frequency shows a linear positive trend like *case a* as the temperature increases up to 25 °C and then undergoes a sudden decay for further increases in the thermal load. The second and third frequencies feature instead an increasing trend up to about 30 °C and are characterized by a very high gradient compared to the corresponding frequencies of the vault with uniform thermal load (Table 2). Finally, the fourth frequency increases until 30 °C and only slightly decreases therefrom. This different behaviour likely depends on the fact that the extension of the cracked regions located at the base of lateral walls and at the keystone and springing sections of the vault grows for lower temperatures. In contrast, as the temperature increases, the distribution of thermal loads facilitates the closure of some cracks as the material expands, contributing to stiffer areas (Fig. 4).

Regardless of the thermal load distribution, the mode shapes show very little sensitivity to thermal variations, as evidenced by the MAC

Table 4

Case a: natural frequencies of the reinforced vault at ϑ_0 (f_0), ϑ_1 (f_1) and ϑ_2 (f_2); relative frequency variation $\Delta f_1 = (f_1 - f_0)/f_0$ and $\Delta f_2 = (f_2 - f_0)/f_0$; MAC value between the mode shapes ϕ_{0i} (i = 1…4) at ϑ_0 and the corresponding ones at ϑ_1 (MAC$_1$) and ϑ_2 (MAC$_2$) for different values of preload force Np.

Mode shape	f_0 [Hz]	f_1 [Hz]	Δf_1 [%]	MAC$_1$ [-]	f_2 [Hz]	Δf_2 [%]	MAC$_2$ [-]
Np = 0 N							
ϕ_1	2.355	2.266	−3.79	0.999	2.333	−0.93	1.000
ϕ_2	9.800	9.727	−0.74	0.999	9.713	−0.88	1.000
ϕ_3	10.653	10.410	−2.28	0.999	10.020	−5.94	0.999
ϕ_4	11.263	10.625	−5.67	0.979	10.973	−2.57	0.998
Np = 1500 N							
ϕ_1	2.398	2.312	−3.61	1.000	2.395	−0.11	1.000
ϕ_2	10.055	10.027	−0.27	0.999	10.036	−0.19	1.000
ϕ_3	11.553	10.673	−7.62	0.984	11.515	−0.33	1.000
ϕ_4	12.044	11.928	−0.96	0.998	11.994	−0.42	1.000
Np = 5000 N							
ϕ_1	2.507	2.426	−3.21	1.000	2.495	−0.46	1.000
ϕ_2	10.868	10.755	−1.04	0.999	10.783	−0.79	1.000
ϕ_3	11.903	10.925	−8.22	0.992	11.896	−0.06	1.000
ϕ_4	13.173	12.327	−6.42	0.931	13.123	−0.38	1.000
Np = 10000 N							
ϕ_1	2.516	2.418	−3.90	1.000	2.517	0.04	1.000
ϕ_2	11.067	10.840	−2.05	1.000	11.069	0.01	1.000
ϕ_3	11.904	10.994	−7.64	0.992	11.907	0.03	1.000
ϕ_4	13.371	12.301	−8.01	0.934	13.376	0.04	1.000
Np = 15000 N							
ϕ_1	2.446	2.314	−5.39	1.000	2.454	0.33	1.000
ϕ_2	10.798	10.511	−2.65	1.000	10.830	0.30	1.000
ϕ_3	11.802	10.976	−7.00	0.989	11.814	0.10	1.000
ϕ_4	12.782	11.985	−6.24	1.000	12.874	0.72	1.000

values, which are close to the unit over the entire temperature interval, thus confirming the experimental results observed in [15,16,23].

3.2. A barrel vault on lateral walls constrained by steel tie rods

The second example under investigation is the barrel vault described above reinforced with two steel tie rods having a square section of 0.01 m edge (Fig. 5). The FE model of the structure now comprises 1288 thick shell and beam elements (elements no. 10 and 9), respectively, of the NOSA-ITACA library [48], for a total of 1417 nodes and 8502 degrees of freedom. The beams modelling the tie rods are connected to the shell elements via multipoint constraint relations to be activated when the masonry structure is in equilibrium under self-weight. The two tie rods are preloaded by a tensile force Np of variable amplitude. As done in the previous section, two different temperature distributions are considered: a uniform thermal load (*case a*) and a linear thermal load (*case b*) through the elements' thickness.

Once again, the analyses are performed assuming that both the vault and the lateral walls are made of a masonry-like material while the tie-rods, made of steel, have a linear elastic behaviour. The mechanical properties of the materials, summarized in Table 3, do not vary with temperature ϑ. The reference temperature ϑ_0 is set always equal to 20 °C. Each analysis is conducted according to the following sequence: i) application of the structure's self-weight and equilibrium achievement; ii) connection of the tie-rods to the structure and application of beam's self-weight along with a constant tensile preload force Np starting from the stress–strain fields obtained at the previous step; iii) incremental application of the thermal loads (uniform or linear) with ϑ varying in the interval [ϑ_1, ϑ_2] and assuming $\vartheta_1 = 0$ °C and $\vartheta_2 = 35$ °C, respectively; iv) calculation, after each thermal load increment, of natural frequencies f_i (ϑ), mode shapes (for i = 1,…,4) and MAC values between current mode shapes and those corresponding to the reference temperature ϑ_0. The previous steps are repeated for different choices of Np, which is supposed to vary within the interval [0,15000] N (the upper limit adopted indicates a reasonably high stress level of $1.50 \bullet 10^8$ Pa, still before

yielding).

Fig. 6 depicts the first four mode shapes of the system, estimated at the reference temperature, with varying values of preload force applied to the tie-rods. With reference to the same modes and for each value of Np, Fig. 7 shows the frequencies and MAC values trends with increasing temperature in case of uniform thermal load distribution, while Fig. 8 shows the norm of the fracture strain tensor obtained at the reference temperature and at the bounds of the temperature range. Table 4 lists, for each value of preload force, the structure's natural frequencies at ϑ_0 (f_0), ϑ_1 (f_1) and ϑ_2 (f_2); the relative frequency variation against the reference temperature scenario $\Delta f_1 = (f_1 - f_0)/f_0$ and $\Delta f_2 = (f_2 - f_0)/f_0$, as well as the MAC values calculated between the mode shapes ϕ_{0i} at ϑ_0 and the corresponding ones at ϑ_1 (MAC$_1$) and ϑ_2 (MAC$_2$). The analysis of these figures and Table 4 allows to draw the following remarks:

- at the reference temperature, the first two mode shapes of the reinforced vault involve a global translation in X direction and a vertical flexural bending in Z direction, and remain unchanged as the force Np varies; the third mode shape is a bending mode in X direction that mainly involves the vault (recalling the first asymmetrical mode shape typical of arches) when Np is equal to zero, but it becomes a torsional mode around the Z-axis for higher values of preload; whereas, the fourth mode shape varies as a function of the Np applied to tie rods, featuring either a torsional configuration symmetrical with respect to the YZ plane of the vault or a bending configuration in X direction mainly involving the vault. It is noteworthy that variations in the mode shape sequences are not uncommon in this type of structures as already demonstrated in [50];
- overall, mode shapes are less sensitive than frequencies to thermal variations for any value of tie-rods preload;
- for a fixed temperature value, the frequency values increase as the preload force Np rises up to 10000 N and then frequency values decrease. This trend can be explained by observing the evolution of the crack pattern of the vault under uniform thermal load distributions: in fact, the micro-fractures at the intrados section of the vault's keystone and at the extrados of the springing sections progressively close until a preload force equal to 10000 N; for higher values of Np, new micro-cracks open up in a different area;
- regardless of the preload force, all the frequencies increase with rising temperatures up to 15 °C, remaining almost constant therefrom (except for modes 3 and 4 in case of Np = 0 where frequencies show a decreasing trend after 20 °C). This behaviour is likely due to the fact that for temperatures above 15 °C all the cracks are closed, the structure has a linear elastic behaviour, and only for some values of Np an increase in temperature corresponds to the opening of new cracks.

Fig. 9 shows, for the first four mode shapes of the structure and for each value of preload force Np, the evolution of frequencies and MAC values with increasing temperature in case of linear thermal load through the elements' thickness. Fig. 10 depicts the norm of the fracture tensor, for each value of Np, both at the reference temperature and at the bounds of the considered temperature range. For comparative purposes, Table 5 lists the structure's natural frequencies at ϑ_0 (f_0), ϑ_1 (f_1) and ϑ_2 (f_2) for increasing values of preload force, together with the relative frequency variation against the reference temperature scenario $\Delta f_1 = (f_1 - f_0)/f_0$ and $\Delta f_2 = (f_2 - f_0)/f_0$ and the MAC values calculated between the mode shapes ϕ_{0i} at ϑ_0 and the corresponding ones at ϑ_1 (MAC$_1$) and ϑ_2 (MAC$_2$). The observation of the figures and Table 5 allows one to underline the following aspects:

- for any value of tie-rods preload, mode shapes are always less sensitive than frequencies to thermal variations even in the case of linear thermal load distribution through the elements' thickness. This outcome corroborates the experimental evidence [12,15];
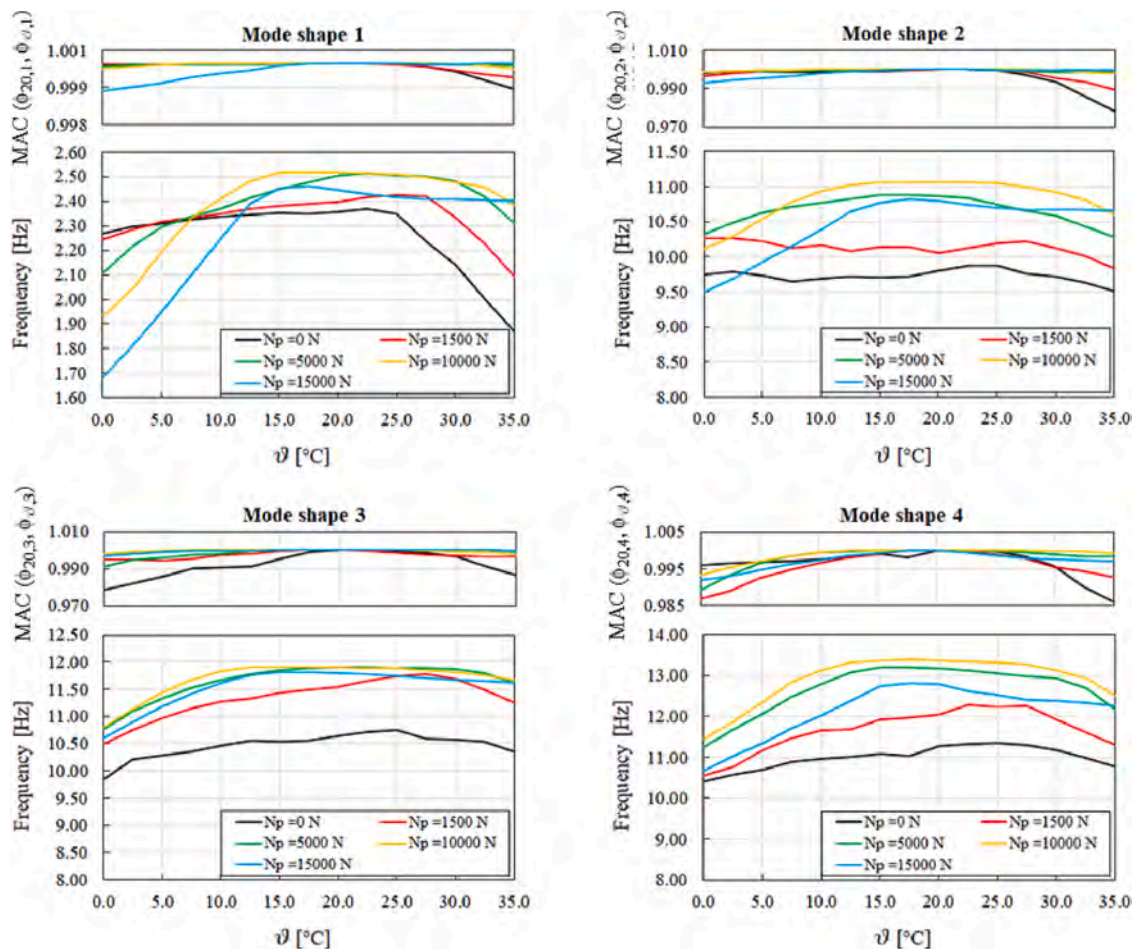
Fig. 9. Evolution of frequencies and MAC values of the reinforced vault mode shapes with varying temperature for different values of Np in case of linear thermal load applied to the structure. Note the different vertical scales used. (For interpretation of the references to colour in this figure legend, the reader is referred to the web version of this article).

- for any temperature value, the frequency values increase as the preload force Np rises up to a value of 10000 N and then frequency values decrease. This behaviour can be explained by observing that the evolution of the crack pattern of the vault under linear thermal load distribution: indeed, the micro-fractures of the structure progressively close until the preload force is equal to 10000 N; then, for higher values of Np, new micro-cracks open up;
- particularly, the first frequency shows a greater sensitivity to temperature variations as compared to the case of constant thermal load. If the preload force is less than 5000 N, the frequency slowly increases with growing temperatures up to 20–25 °C; from that value onwards, it reduces abruptly. This is because the linear thermal variation induces a flexion in the lateral walls, leading to the closure of micro-cracks at the base of the walls and to the reduction of fractures at the vault impost area; yet, for temperatures above 20 °C, new cracks open at the vault keystone and the base of the lateral walls. For preload force greater than 5000 N, the turning point between increasing and decreasing frequency moves towards lower temperature values (15 °C) and the overall trend changes radically; indeed, for temperatures increasing from 0 °C to 15 °C, frequencies quickly rise as a result of some fractures closure at the structure's extrados; whereas, for temperature values higher than 15° C, the natural frequencies of the reinforced vault either remain constant or slowly decrease due to the opening of some new cracks at the intrados section of the vault impost;
- the second frequency, for values of preload Np below 5000 N, does not show a clear trend as a function of temperature; this is because

the second mode shape features a vertical bending configuration which mainly involves the vault whose fractures do not vary significantly as a function of the applied thermal load (the keystone is permanently characterized by micro-cracks). Conversely, for preloads higher than 5000 N, at the reference temperature, the structure appears intact (no fracture deformations) due to the beneficial effect of Np. In the range 0°-15 °C, the frequency increases with progressive temperature but, once the value of 15° C is exceeded, it remains constant or decreases due to the occurrence of new cracks across the vault and at the base of the lateral walls. An exception is the case with preload Np = 15000 N, which corresponds to a widely diffused crack pattern in the structure at 0 °C, and a more localized crack pattern at the springing of the vault at 35 °C; accordingly, the frequency of this mode rapidly increases as the temperature rises up to 15 °C and then it stabilizes and remains nearly constant;
- the considerations made hitherto can be also extended to the higher frequencies of the vault (i.e., the frequencies of modes 3 and 4).

4. Application to the Mogadouro clock tower, in Portugal

The full five step procedure outlined in Section 2 for the simulation of the dynamic behaviour of a monitored masonry structure subjected to temperature variation is here applied to a real benchmark case study: the Mogadouro clock tower in Portugal (Fig. 11). The 20.4 m high tower, built after 1559, has a rectangular cross section, 4.7 × 4.5 m², and is made of three-leaf large block granite masonry walls with rubblestone inner core and a total thickness of about 1 m. Due to its severe state of
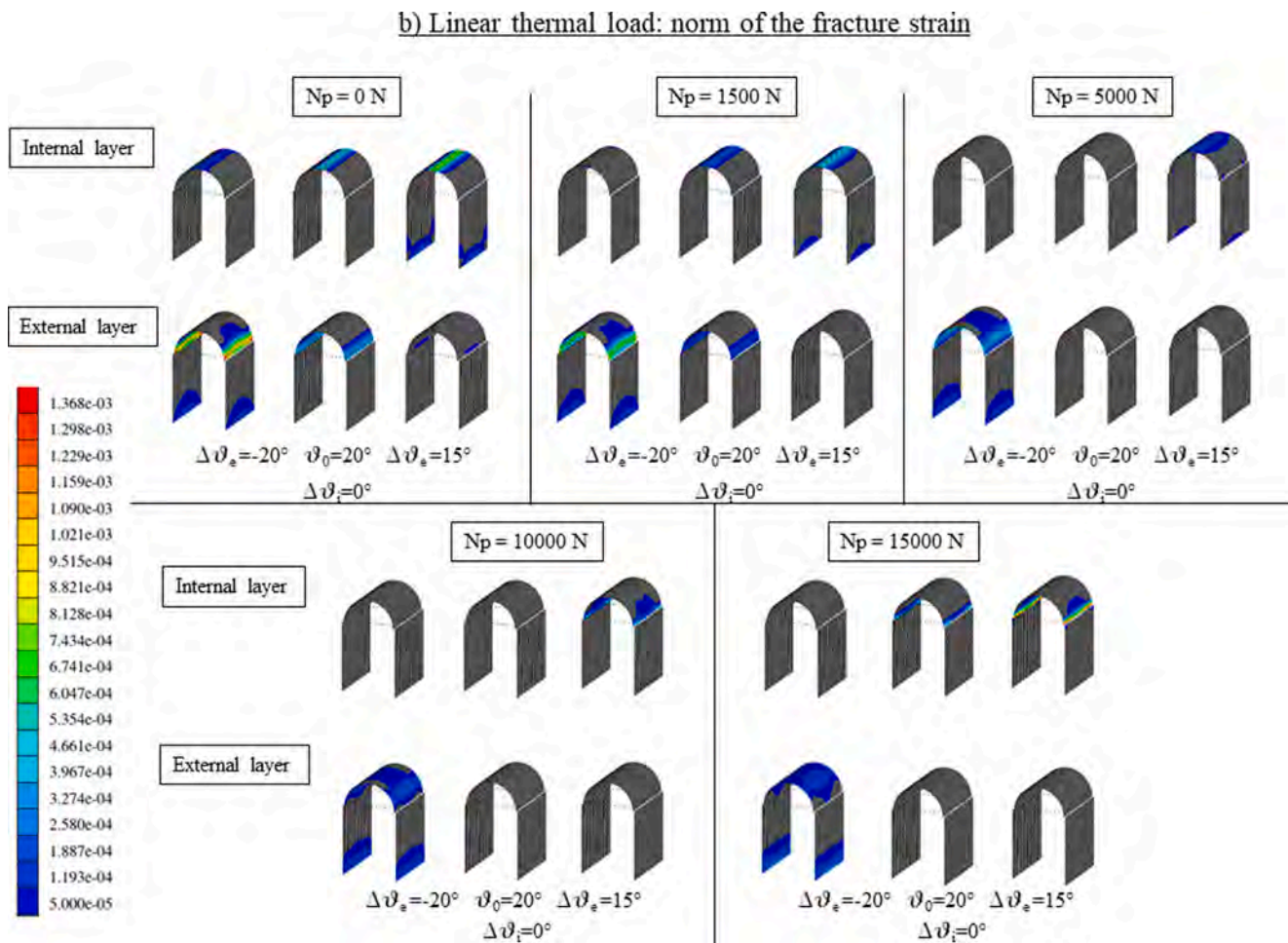
b) Linear thermal load: norm of the fracture strain

Fig. 10. Crack pattern in the vault for different values of Np under linear thermal load distributions in the configurations corresponding to the reference temperature ϑ_0 (20 °C) and to the lower and upper bounds of the temperature variation range [ϑ_1, ϑ_2]. (For interpretation of the references to colour in this figure legend, the reader is referred to the web version of this article).

decay, repair and strengthening works were carried out in 2005, comprising mostly lime-based injections and installation of an upper steel ring using external profiles. Steps a., b. and c. of the procedure presented in this work, which are concerned with the preliminary dynamic identification tests and the long-term acquisition for modal and temperature tracking, have been thoroughly discussed in [30]. Monitoring was carried out between April 2006 and December 2007 in the strengthened structure. Fig. 12 shows the experimental trend of the frequency values for the first four modes of the towers, hereafter used for calibration and comparison purposes, corresponding to the first bending modes along two horizontal directions (modes 1 and 2), torsion (mode 3) and second bending mode along one direction (mode 4). An evident shift of about 4% in the frequency trend emerges in the records of modes 1 and 2, giving rise to a double cluster in their frequency-temperature correlation plots. This peculiar behaviour has been explained as the effect of humidity and water absorption from the tower's walls at the beginning of the rainy season [30] and is further discussed in the following analyses.

As concerns steps d. and e. of the procedure, a FE model of the structure is built using 18,024 isoparametric 8-node brick elements to discretize the walls and 352 thick shell elements to discretize the roof, counting a total of 23,467 nodes (Fig. 13). The tower is assumed to be clamped at the base (no information related to the foundations and the soil are available, so the soil structure interaction is neglected) and constituted by linear elastic materials as far as the roof (material no. 5) and top pillars (material no. 4) are concerned, and masonry-like materials in what concerns South and North façades (material no. 1), East and West façades (material no. 2), and walls' corners (material no. 3). The choice of linear elastic materials to model pillars and roof stems from the observation that these elements do not affect the overall dynamic behaviour of the tower. Indeed, the low elastic modulus adopted for the roof allows the tower cross section to deform freely within its own plane in agreement with the experimental evidence [51].

To investigate how variations in the masonry mechanical properties (Young's moduli and tensile strength) influence the output of the numerical model (the natural frequencies), a preliminary Global Sensitivity Analysis (GSA) has been performed through the SAFE Toolbox [52]. The SAFE Toolbox, an open–source code implemented in MATLAB, can be easily linked to simulation models running outside the MATLAB environment, such as the NOSA-ITACA code in the example at hand. The Elementary Effects Test (EET method [53]) is used to evaluate the sensitivity indices assuming that the four input parameters (tensile strength and Young's moduli of materials 1, 2 and 3) have a uniform probability distribution function, and adopting the Latin Hypercube method [54] as sampling strategy. From Fig. 14, where the sensitivity indices calculated via the EET method are plotted, it is possible to deduce that the Young's moduli of materials 1, 2 and 3 affect the numerical frequencies much more than the tensile strength, and in particular those associated with the higher order mode shapes.

The (optimal) mechanical properties of the materials 1, 2 and 3 are then estimated via the nonlinear model updating procedure recalled in Section 2 and described in [43].

Table 5

Case b: natural frequencies of the reinforced vault at ϑ_0 (f_0), ϑ_1 (f_1) and ϑ_2 (f_2); relative frequency variation $\Delta f_1 = (f_1 - f_0)/f_0$ and $\Delta f_2 = (f_2 - f_0)/f_0$; MAC value between the mode shapes ϕ_{0i} (i = 1,...,4) at ϑ_0 and the corresponding ones at ϑ_1 (MAC$_1$) and ϑ_2 (MAC$_2$) for different values of Np.

Mode shape	f_0 [Hz]	f_1 [Hz]	Δf_1 [%]	MAC$_1$ [-]	f_2 [Hz]	Δf_2 [%]	MAC$_2$ [-]
Np = 0 N							
ϕ_1	2.355	2.271	−3.59	1.000	1.867	−20.74	0.999
ϕ_2	9.800	9.740	−0.61	0.998	9.507	−2.99	0.978
ϕ_3	10.653	9.850	−7.53	0.978	10.351	−2.84	0.986
ϕ_4	11.263	10.395	−7.71	0.996	10.759	−4.47	0.986
Np = 1500 N							
ϕ_1	2.398	2.244	−6.42	1.000	2.094	−12.67	0.999
ϕ_2	10.055	10.266	2.10	0.997	9.834	−2.20	0.990
ϕ_3	11.553	10.494	−9.17	0.995	11.263	−2.51	0.996
ϕ_4	12.044	10.554	−12.37	0.987	11.295	−6.22	0.993
Np = 5000 N							
ϕ_1	2.507	2.110	−15.81	1.000	2.309	−7.91	1.000
ϕ_2	10.868	10.314	−5.10	0.999	10.274	−5.47	0.999
ϕ_3	11.903	10.766	−9.56	0.991	11.617	−2.41	0.999
ϕ_4	13.173	11.255	−14.56	0.989	12.156	−7.72	0.998
Np = 10000 N							
ϕ_1	2.516	1.934	−23.15	1.000	2.384	−5.27	1.000
ϕ_2	11.067	10.109	−8.66	0.998	10.602	−4.20	0.998
ϕ_3	11.904	10.811	−9.18	0.998	11.665	−2.01	0.998
ϕ_4	13.371	11.441	−14.44	0.993	12.489	−6.59	0.999
Np = 15000 N							
ϕ_1	2.446	1.685	−31.10	0.999	2.402	−1.79	1.000
ϕ_2	10.798	9.489	−12.13	0.993	10.655	−1.33	0.999
ϕ_3	11.802	10.602	−10.17	0.997	11.614	−1.59	1.000
ϕ_4	12.782	10.663	−16.58	0.992	12.262	−4.07	0.997

For the present case study, the reference temperature ϑ_0 is assumed equal to 17 °C, corresponding to the average temperature value of the monitoring period and a thermal expansion coefficient α equal to $5 \bullet 10^{-6}$ (°C)$^{-1}$ is assumed for the whole structure, as suggested in pertinent literature works about historical masonry [55,56].

The nonlinear model updating assumes that the Poisson's ratio ν of all materials as well as the mechanical characteristics of materials 4 and 5 are fixed and the tower is subjected solely to the self-weight load.

The FE model of the tower has been calibrated by using four experimental frequencies ($q = 4$), four unknown parameters ($p = 4$) and setting in Eq. (2) $w_i = f_{i,exp}^{-1}$. In order to obtain a numerical model close to reality, the first four experimental frequencies $f_{0,exp}^1$ (or reference dynamic properties) used for the calibration, and listed below, are estimated considering the mean of the values at the reference temperature ϑ_0 in cluster 1:

$$f_{0,exp}^1 = [2.503, 2.706, 7.001, 8.581].$$

The parameters to be updated are the tensile strength σ_t (assumed the same for the whole structure) and the Young's modulus E_0^1 (for i = 1...3) of masonry materials 1, 2 and 3 (Table 6) varying within the ranges defined by their lower and upper bounds as follows:

$$0.0 \leq \sigma_t \leq 5 \bullet 10^5 \text{ Pa}, \quad 0.5 \bullet 10^9 \leq E_{0,i}^1 \leq 5.5 \bullet 10^9 \text{ Pa (i = 1...3)} \tag{3}$$

Table 6 reports the optimal values of the mechanical characteristics obtained by nonlinear model updating; Table 7 summarizes the results in terms of experimental ($f_{0,exp}^1$) and numerical ($f_{0,N}^1$) frequencies, relative frequency percentage error, and MAC values between experimental and numerical mode shapes (cluster 1). The first two frequencies of the tower and associated mode shapes are very well approximated, with relative frequency errors close to zero and a high degree of consistency between the modal displacements of the fundamental modes. The approximation for the higher modes is slightly less accurate, particularly for the torsional mode (mode 3), with a maximum relative frequency error of 5.4%. Given the greater degree of complexity characterizing experimental high-frequency modes [57], the outcome of the model updating procedure is more than satisfactory. Yet, for the purpose of this work, the following analysis will focus mostly on the two first fundamental modes of the tower.

Fig. 15 provides a graphic representation of the objective function Φ defined on the 4-dimensional box Ω, given in (3), with real values. For some assigned tensile strength values, it shows the plot of the objective function given in Eq. (2) in the log-scale, as the three elastic moduli vary. Furthermore, each diagram reports the value of Young's moduli at which the objective function reaches its minimum value Φ_{min}. The Figure confirms that the solution identified by the algorithm (corresponding to the second plot with Φ_{min} and the value of the minimum point in bold) is the global minimum point.

Once the optimal values of the constituent materials are estimated, the dynamic properties of the tower are calculated as a function of the

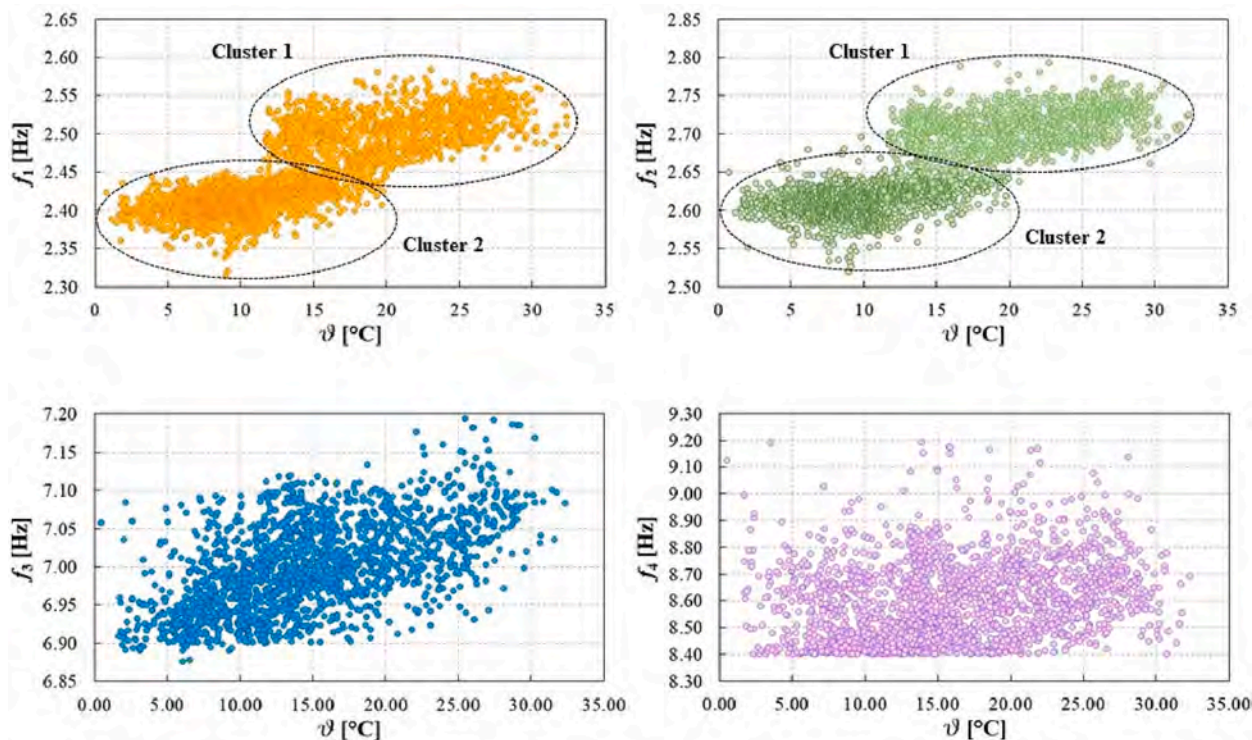**Fig. 11.** Mogadouro castle (left) and the clock tower (right).

Fig. 12. Experimental trend of the first four modes of the Mogadouro clock tower with the identification of the two clusters in frequency 1 and 2. (For interpretation of the references to colour in this figure legend, the reader is referred to the web version of this article).
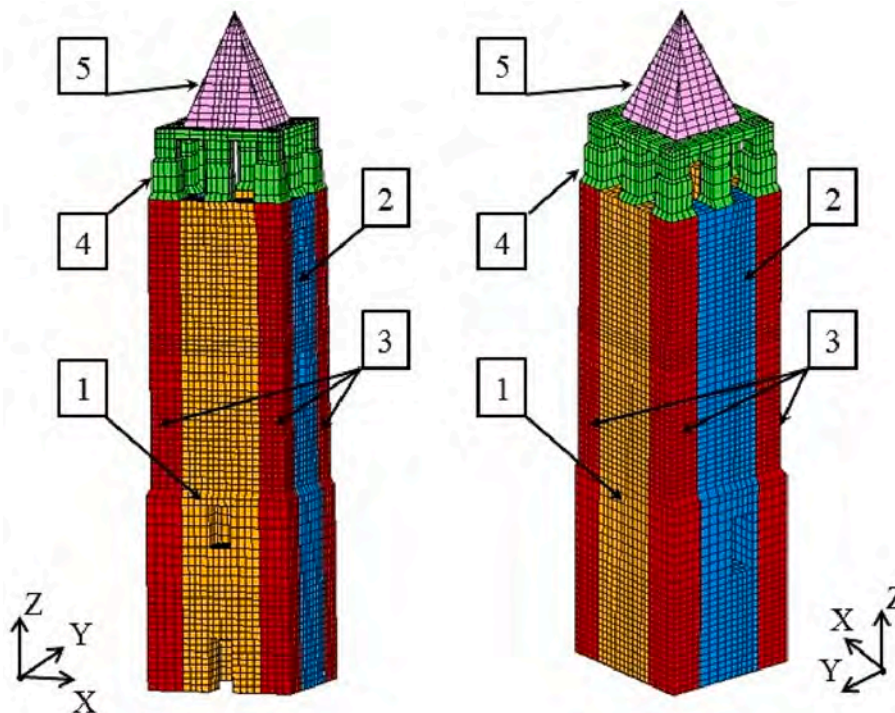

Fig. 13. FE model of the Mogadouro tower with indication of the constituent materials (different colours and label number).

temperature variations recorded experimentally in cluster 1.

Incremental uniform thermal loads are applied to the FE model up to a maximum temperature $\vartheta_{max} = 29\ °C$ (extreme values are disregarded because less representative of the considered temperature range). After each increment, the first two natural frequencies and mode shapes of the tower are calculated via the linear perturbation analysis implemented in

NOSA-ITACA and the MAC values between the current mode shapes and those corresponding to the reference temperature are estimated.

Fig. 16 shows, in the upper part for cluster 1, the experimental trend of the first (left side in orange) and of the second (right side in green) frequency along with their numerical counterparts (rhomboid black dots). The rhomboid black dots without filling (in cluster 1) represent
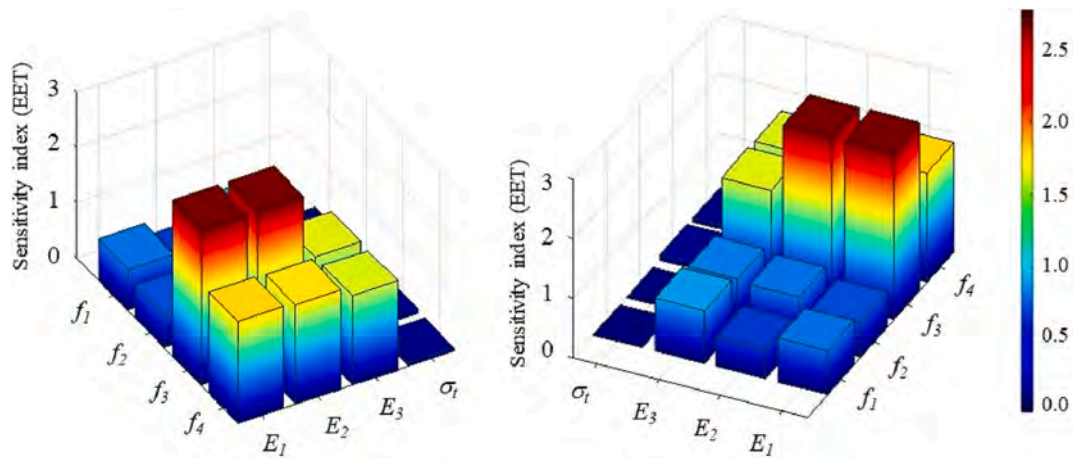
Fig. 14. EET sensitivity indices for the first four frequencies and four parameters. (For interpretation of the colours in this figure legend, the reader is referred to the web version of this article).

Table 6
Optimal values of the material mechanical properties.

Material	Tower's portion	ν [-]	ρ[kg/ m^3]	E_0^1 [Pa]	σ_t [Pa]	α[°C^{-1}]
1	South and North Façades	0.2	2200	1.760•10^9	11,000	5•10^{-6}
2	East and West Façades	0.2	2200	0.810•10^9	11,000	5•10^{-6}
3	Walls' Corners	0.2	2400	4.960•10^9	11,000	5•10^{-6}
4	Top Pillars	0.2	2200	1.210•10^9	–	5•10^{-6}
5	Roof	0.2	2000	0.195•10^9	–	5•10^{-6}

Table 7
Cluster 1: Comparison between experimental ($f_{0,exp}^1$) and numerical frequencies ($f_{0,N}^1$); relative frequency error $\Delta f_0^1 = (f_{0,exp}^1 - f_{0,N}^1)/ f_{0,exp}^1$ and MAC[1] values between corresponding mode shapes.

Mode shape	$f_{0,exp}^1$ [Hz]	$f_{0,N}^1$ [Hz]	Δf_0^1 [%]	MAC[1]
1	2.503	2.502	0.04	0.98
2	2.706	2.716	−0.37	0.98
3	7.001	6.624	5.38	0.97
4	8.581	8.311	3.15	0.74

the extrapolation of the numerical simulation with the cluster 2 neglected. At the bottom, Fig. 16 depicts the percentage relative error trend calculated between the numerical and the corresponding experimental frequencies estimated by resorting to the regression line equation. Fig. 17 and Fig. 18 report the fracture strain patterns of Mogadouro clock tower corresponding, respectively, to the reference temperature ϑ_0 and the maximum reached temperature ϑ_{max}.

It is clear from the plots that the numerical algorithms implemented are able to capture the variations of the dynamic properties of the masonry structure as a function of the temperature until 20 °C: indeed, up to this value, the numerical frequencies slightly increase, but then they remain constant till 29 °C. This behaviour does not fully reflect the experimental evidence where a direct frequency-temperature correlation is found for the entire period. This phenomenon is directly related to the crack pattern exhibited by the model at the different temperatures ϑ_0 and ϑ_{max} which is practically unchanged; the discretized structure expands freely and the existing micro fractures remain the same (Fig. 17 and Fig. 18). Although the interior of the tower is not thermally isolated from exogenous factors, a linear temperature distribution through the tower walls' thickness was also considered. The results obtained coincide with those of uniform temperature distribution, without making any improvements to the modelling, thus for the sake of brevity they are

not reported in the paper.

Aiming at following the dynamic behaviour of Mogadouro clock tower across the entire temperature interval, the frequency trends in the second cluster must be considered as well. To this end, it is necessary to catch the frequency gap observed in the experimental data between the two identified clusters that, as already mentioned, is likely due to the humidity and water absorption during the rainy season. As well-known in the literature, the influence of moisture inside masonry walls can result either into a mass increase [58] or a stiffness decrease [59,60]. Since NOSA-ITACA does not allow to directly consider the humidity variation within the masonry, its effect is artificially introduced in the numerical simulations considering the humidity effect through a stiffness decrease [59,60]. Hence, a new nonlinear model updating has been performed considering the same parameters of the optimization process followed for cluster 1, the same variation ranges and the mean value of the experimental frequencies at 17 °C of cluster 2:

$$f_{0,exp}^2 = [2.432, 2.634, 6.993, 8.476].$$

Table 8 summarizes the results of the optimization process in terms of elastic moduli, resulting in a reduction of about 6–7% with respect to the values obtained for cluster 1; the tensile strength value remains unchanged.

Table 9 summarizes the results obtained for the FE model of the tower at the reference temperature scenario ϑ_0 for cluster 2 in terms of experimental ($f_{0,exp}^2$) and numerical ($f_{0,N}^2$) frequencies, relative frequency error, and MAC values between experimental and numerical mode shapes. Once again, the first two frequencies and the mode shapes of the structure are very well approximated, while higher frequency errors are found for modes 3 and 4, reading a maximum relative percentage error of 8.2% for the frequency of the third mode.

After concluding this second calibration process, the dynamic properties of the tower are calculated as a function of the temperature variations recorded experimentally in cluster 2. Uniform decreases in temperature are applied up to a minimum temperature of 2 °C. As done for cluster 1, after each temperature decrease, the first two natural frequencies and mode shapes of the tower are calculated via the linear perturbation analysis implemented in NOSA-ITACA and the MAC values between the current mode shapes and those corresponding to the reference temperature are estimated. Fig. 16 shows, in the upper part for cluster 2, the experimental trend of the first (left side in orange) and of the second (right side in green) frequency versus the numerical counterpart. For comparative purposes, the trend obtained for cluster 1 data is overlapped as well. At the bottom, Fig. 16 depicts the percentage relative error trend calculated between the numerical and the corresponding experimental frequencies estimated by resorting to the
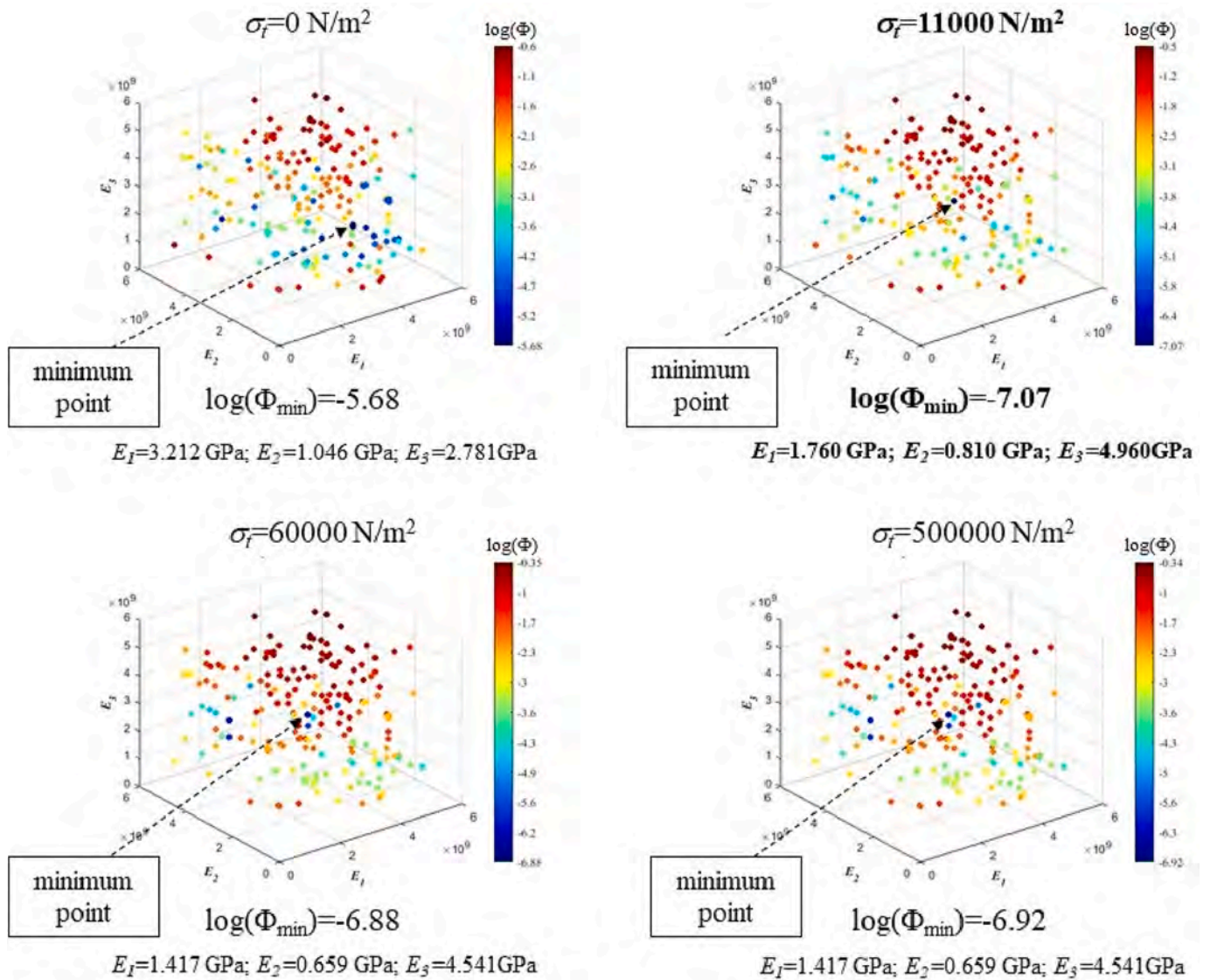
Fig. 15. Value of the objective function defined in Eq. (2) calculated as the unknown parameters vary.
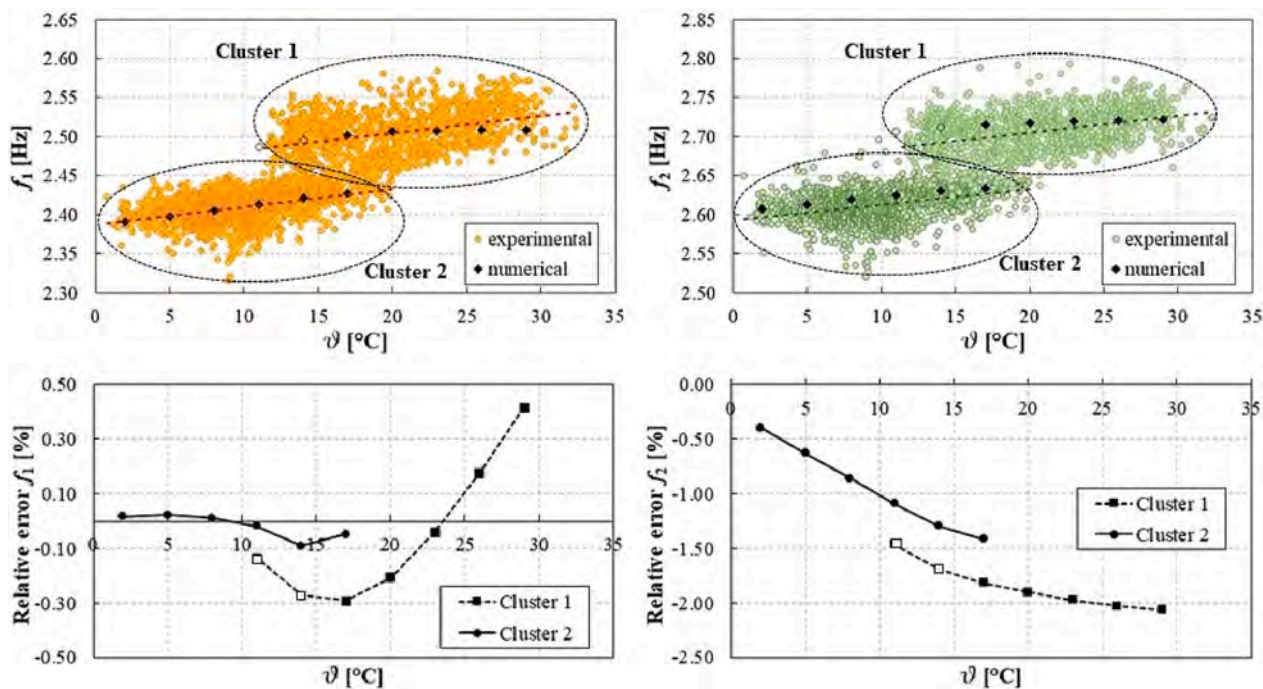
Fig. 16. Up: Experimental (circular dots) versus numerical (rhomboid black dots) trend. Bottom: Relative error between the interpolated values of the experimental frequencies (on the regression line) and the numerical counterparts. (For interpretation of the references to colour in this figure legend, the reader is referred to the web version of this article.).
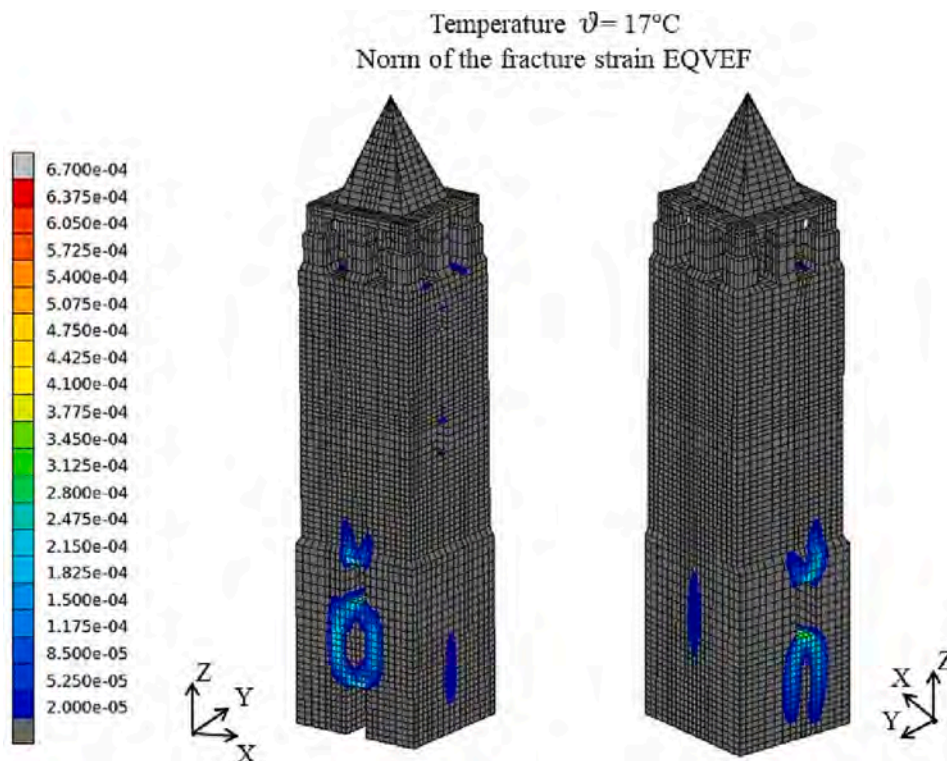

Fig. 17. Pattern of fracture strain norm at the reference temperature ϑ_0. (For interpretation of the references to colour in this figure legend, the reader is referred to the web version of this article).

regression line equation. Fig. 19 depicts the fracture strain pattern of Mogadouro clock tower corresponding to a temperature value of 2 °C.

In this case, the numerical model is able to satisfactorily reproduce the actual dynamic behaviour of the structure across the entire temperature interval, exhibiting the same frequency-temperature trend observed experimentally for cluster 2, i.e. decreasing frequencies as the temperature decreases and vice versa. Indeed, as observed in Fig. 19, new cracks arise at the base of the tower at 2 °C and the size of the cracks
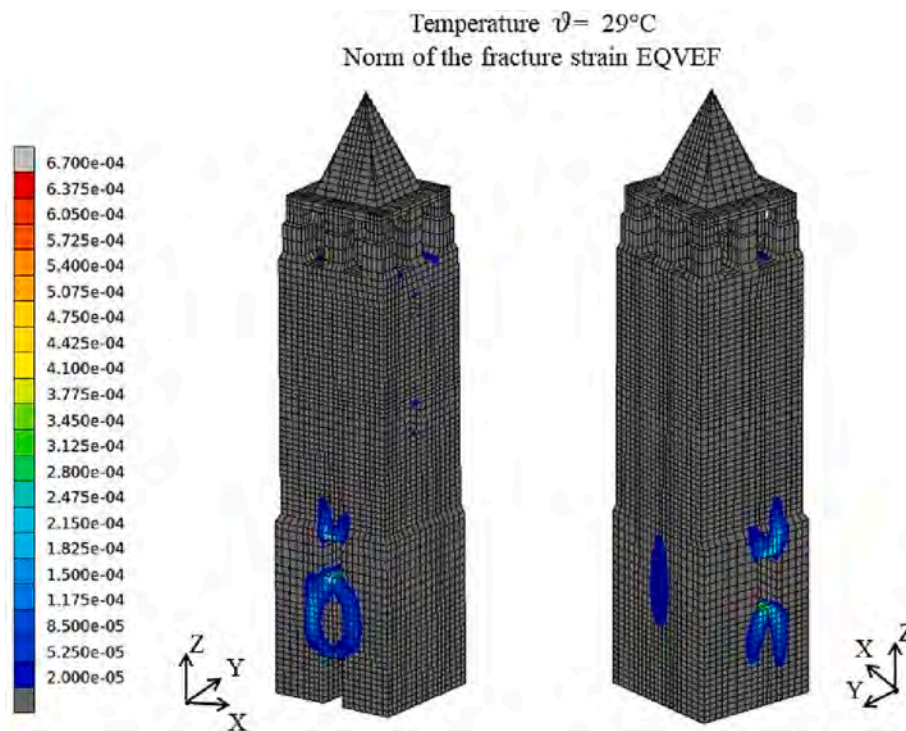
Fig. 18. Pattern of fracture strain norm of the tower at temperature ϑ_{max}. (For interpretation of the references to colour in this figure legend, the reader is referred to the web version of this article).

Table 8
Young's moduli used in the numerical simulations for both cluster 1 and cluster 2.

Material	Tower's portion	E_0^1 [N/mm^2]	E_0^2 [N/mm^2]	E_0^2/E_0^1
1	South and North Façades	$1.760 \cdot 10^9$	$1.640 \cdot 10^9$	0.932
2	East and West Façades	$0.810 \cdot 10^9$	$0.764 \cdot 10^9$	0.943
3	Walls' Corners	$4.960 \cdot 10^9$	$4.670 \cdot 10^9$	0.941
4	Top Pillars	$1.210 \cdot 10^9$	$1.210 \cdot 10^9$	1.000
5	Roof	$0.195 \cdot 10^9$	$0.195 \cdot 10^9$	1.000

Table 9
Cluster 2: Comparison between experimental ($f_{0,exp}^2$) and numerical frequencies ($f_{0,N}^2$); relative frequency error $\Delta f_0^2 = (f_{0,exp}^2 - f_{0,N}^2)/f_{0,exp}^2$ and MAC^2 values.

Mode shape	$f_{0,exp}^2$ [Hz]	$f_{0,N}^2$ [Hz]	Δf_0^2 [%]	MAC^2
1	2.432	2.427	0.21	0.98
2	2.634	2.634	0.00	0.98
3	6.993	6.422	8.17	0.97
4	8.476	8.121	4.19	0.74

already existing at the reference temperature (see Fig. 17) tends to increase, leading to frequency downshifts. It is worth noting that the same numerical results have been obtained considering an increase of mass instead of a decrease of stiffness to simulate the humidity effect in the tower. For the sake of brevity, these results are not reported.

5. Conclusions

The paper presents a numerical investigation of the effects of temperature variation on masonry structures' static and dynamic behaviour. The influence of temperature is assessed by resorting to a finite element code (NOSA-ITACA, https://www.nosaitaca.it/software/) able to model the peculiar constitutive behaviour of masonry under static, dynamic and thermal loads. The effects of thermal variation over the modal properties of a masonry structure are evaluated via a linear perturbation procedure. The investigation is carried out on two trial examples (a masonry portal with and without tie-rods reinforcement). The code is then applied to a real case study, the Mogadouro tower, which has been the subject of a long-term dynamic monitoring campaign, whose results highlighted the dependence of the first two tower's natural frequencies on temperature.

The primary outcomes of the paper can be summarized as follows.

- The code can model the effects of the crack pattern in the static and dynamic behaviour of a masonry structure.
- Temperature variations affect a masonry structure's static and dynamic behaviour because they induce changes in the stress field and in the crack distribution over the structure.
- The Mogadouro tower shows a positive correlation between the two first frequencies and temperature, as evidenced in different long-term dynamic monitoring campaigns.
- The experimental results of the Mogadouro tower monitoring campaign show a peculiar behaviour likely attributed to yearly changes in the moisture content of the masonry walls.
- The code is able to reproduce the results of the Mogadouro experiment, with regard to the effects of temperature variations on the modal properties of the tower with a maximum relative error of about 0.4% for the first frequency and 2% for the second one considering the experimental frequencies estimated by linear regression.
- The code cannot directly reproduce the influence of humidity on the modal properties of Mogadouro's tower; in the present paper, it is modelled by assuming a reduction of the structural stiffness as shown in the literature.

Further investigations are necessary to validate the procedure, highlight its strengths and weaknesses and gather suggestions on improving or modifying the procedure's phases. Future works that are recommended include: i) development of experimental tests in climate chamber to evaluate the variation of the Young's modulus as a function of the temperature and relative humidity variations for different types of
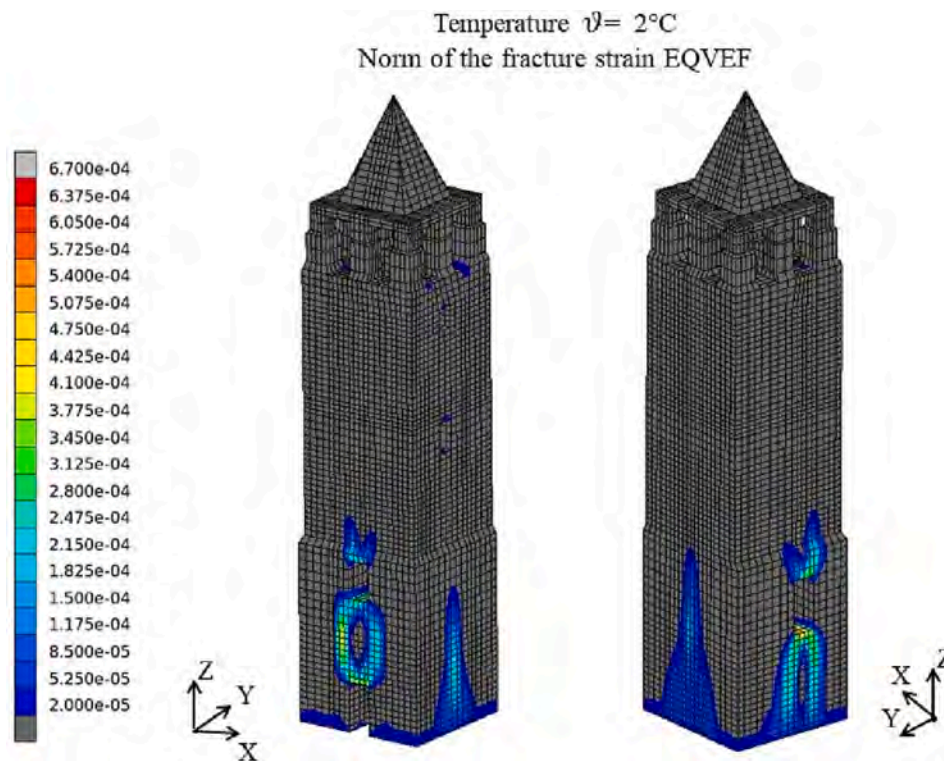
Fig. 19. Pattern of fracture strain norm of the tower at temperature ϑ_{min}. (For interpretation of the references to colour in this figure legend, the reader is referred to the web version of this article).

masonry; ii) construction of masonry mock-ups whose dynamic properties will be evaluated as the climatic conditions and boundary conditions vary; iii) introduction of damage in the specimens; iv) execution of numerical simulations via different FE codes to replicate the experimental results and compare different constitutive equations; v) implementation of new algorithms capable of simultaneously considering the influence of the thermal load and humidity on the dynamic characteristics of the structures.

Declaration of Competing Interest

The authors declare that they have no known competing financial interests or personal relationships that could have appeared to influence the work reported in this paper.

Acknowledgements

References

[1] Guidi, C. Influenza della temperatura sulle costruzioni murarie. Atti della Reale Accademia delle Scienze di Torino (1906) 319–330.

[2] Blasi C, Coisson E. The effects of temperature on historical stone masonry structures. Struct Anal Historic Constr Preserv Saf Sig 2008:1271–6. https://doi.org/10.1201/9781439828229.ch146.

[3] Talebinejad I, Fischer C, Ansari F. A hybrid approach for safety assessment of the double span masonry vaults of the Brooklyn Bridge. J Civ Struct Heal Monit 2011;1 (1–2):3–15. https://doi.org/10.1007/s13349-011-0003-y.

[4] Geimer PR, Finnegan R, Moore JR. Meteorological controls on reversible resonance changes in natural rock arches. J Geophys Res Earth 2022;e2022JF006734. https://doi.org/10.1029/2022JF006734.

[5] Gruber D, Andreev K, Harmuth H. FEM simulation of the thermomechanical behaviour of the refractory lining of a blast furnace. J Mater Process Technol 2004; 155:1539–43. https://doi.org/10.1016/j.jmatprotec.2004.04.249.

[6] Lucchesi, M., Padovani, C., Pasquinelli, G., Zani, N. Masonry constructions: mechanical models and numerical applications (2008); Lecture Notes in Applied and Computational Mechanics. Springer–Verlag. https://doi.org/10.1007/978-3-540-79111-9.

[7] Kita A, Cavalagli N, Ubertini F. Temperature effects on static and dynamic behavior of Consoli Palace in Gubbio. Italy Mech Syst Sig Process 2019;120:180–202. https://doi.org/10.1016/j.ymssp.2018.10.021.

[8] Ceravolo R, Coletta G, Miraglia G, Palma F. Statistical correlation between environmental time series and data from long-term monitoring of buildings. Mech Syst Sig Process 2021;152:107460. https://doi.org/10.1016/j.ymssp.2020.107460.

[9] Azzara RM, Girardi M, Iafolla V, Lucchesi DM, Padovani C, Pellegrini D. Ambient vibrations of age-old masonry towers: results of long-term dynamic monitoring in the historic centre of lucca. Int J Archit Heritage 2021;15(1):5–21. https://doi.org/10.1080/15583058.2019.1695155.

[10] Azzara RM, Girardi M, Iafolla V, Padovani C, Pellegrini D. Long-term dynamic monitoring of medieval masonry towers. Front Built Environ 2020;6:9. https://doi.org/10.3389/fbuil.2020.00009.

[11] Marrongelli, G., Gentile, C., & Saisi, A. Automated modal identification of a historic bell-tower. 10th International Masonry Conference (2018), IMC 2018, 222279, 2344–2355.

[12] Saisi, A., Gentile, C., & Ruccolo, A. Dynamic monitoring of ancient masonry towers: Environmental effects on natural frequencies. 10th International Masonry Conference (2018), IMC 2018, 222279, 2328–2343.

[13] Ubertini F, Comanducci G, Cavalagli N, Laura Pisello A, Luigi Materazzi A, Cotana F. Environmental effects on natural frequencies of the San Pietro bell tower in Perugia, Italy, and their removal for structural performance assessment. Mech Syst Sig Process 2017;82:307–22. https://doi.org/10.1016/j.ymssp.2016.05.025.

[14] Gentile C, Saisi A. Assessment of environmental effects for vibration-based damage detection of historic masonry towers. Multidiscipl Digital Publish Inst Proc 2018;2 (8):441. https://doi.org/10.3390/ICEM18-05324.

[15] Gentile C, Ruccolo A, Canali F. Long-term monitoring for the condition-based structural maintenance of the Milan Cathedral. Constr Build Mater 2019;228: 117101. https://doi.org/10.1016/j.conbuildmat.2019.117101.

[16] Alaggio R, Aloisio A, Antonacci E, Cirella R. Two-years static and dynamic monitoring of the Santa Maria di Collemaggio basilica. Constr Build Mater 2021; 268:121069. https://doi.org/10.1016/j.conbuildmat.2020.121069.

[17] Alaei A, Hejazi M, Vintzilaiou E, Miltiadou-Fezans A, Skłodowski M. Dynamic identification of brick masonry semi-circular arches due to temperature and moisture. Structures 2023;50:148–60. https://doi.org/10.1016/j.istruc.2023.02.022.

[18] Sabia D, Demarie GV, Quattrone A. Structural health monitoring of historic masonry towers: The Case of the Ghirlandina Tower, Modena. In: Geotechnical Engineering for the Preservation of Monuments and Historic Sites III. CRC Press; 2022. https://doi.org/10.1201/9781003308867-10.

[19] Elyamani A, Caselles O, Roca P, Clapes J. Dynamic investigation of a large historical cathedral. Struct Control Health Monit 2017;24(3):e1885. https://doi.org/10.1002/stc.1885.

[20] Gentile, C., Saisi, A., & Cabboi, A. Dynamic monitoring of a masonry tower. 8th SAHC Conference on Structural Analysis of Historical Constructions (2012), Wroclaw, Poland.

[21] Gentile C, Guidobaldi M, Saisi A. One-year dynamic monitoring of a historic tower: Damage detection under changing environment. Meccanica 2016;51(11):2873–89. https://doi.org/10.1007/s11012-016-0482-3.

[22] Gentile C, Saisi A. Ambient vibration testing of historic masonry towers for structural identification and damage assessment. Constr Build Mater 2007;21(6): 1311–21. https://doi.org/10.1016/j.conbuildmat.2006.01.007.

[23] Azzara RM, De Roeck G, Girardi M, Padovani C, Pellegrini D, Reynders E. The influence of environmental parameters on the dynamic behaviour of the San Frediano bell tower in Lucca. Eng Struct 2018;156:175–87. https://doi.org/10.1016/j.engstruct.2017.10.045.

[24] Marotta, A., Ruccolo, A., Beskhyroun, S., Sorrentino, L., Liberatore, D., & Ingham, J. M. Ambient vibration tests on New Zealand unreinforced masonry churches using low cost sensors. Proc., 10th Int. Masonry Conf, 2319–2327 (2018).

[25] Masciotta MG, Roque JCA, Ramos LF, Lourenço PB. A multidisciplinary approach to assess the health state of heritage structures: the case study of the Church of Monastery of Jerónimos in Lisbon. Constr Build Mater 2016;116:169–87. https://doi.org/10.1016/j.conbuildmat.2016.04.146.

[26] Saisi A, Gentile C, Guidobaldi M. Post-earthquake continuous dynamic monitoring of the Gabbia Tower in Mantua. Italy Constr Build Mater 2015;81:101–12. https://doi.org/10.1016/j.conbuildmat.2015.02.010.

[27] Zonno G, Aguilar R, Boroschek R, Lourenço PB. Analysis of the long and short-term effects of temperature and humidity on the structural properties of adobe buildings using continuous monitoring. Eng Struct 2019;196:109299. https://doi.org/10.1016/j.engstruct.2019.109299.

[28] Zonno G, Aguilar R, Boroschek R, Lourenço PB. Experimental analysis of the thermohygrometric effects on the dynamic behavior of adobe systems. Constr Build Mater 2019;208:158–74. https://doi.org/10.1016/j.conbuildmat.2019.02.140.

[29] Tsogka C, Daskalakis E, Comanducci G, Ubertini F. The stretching method for vibration-based structural health monitoring of civil structures. Comput Aided Civ Inf Eng 2017;32(4):288–303. https://doi.org/10.1111/mice.12255.

[30] Ramos LF, Marques L, Lourenço PB, De Roeck G, Campos-Costa A, Roque J. Monitoring historical masonry structures with operational modal analysis: Two case studies. Mech Syst Sig Process 2010;24(5):1291–305. https://doi.org/10.1016/j.ymssp.2010.01.011.

[31] Carpinteri, et al. Numerical assessment of three medieval masonry towers subjected to different loading conditions. J Br Masonry Soc Masonry Int 2006;19 (2).

[32] Taliercio A, Binda L. The basilica of san vitale in ravenna: investigation on the current structural faults and their mid-term evolution. J Cult Herit 2008;8:99–118. https://doi.org/10.1016/j.culher.2006.09.005.

[33] Lucchesi M, Padovani C, Pasquinelli G. Thermodynamics of no-tension materials. Int J Solids Struct 2000;37(45):6581–604. https://doi.org/10.1016/S0020-7683 (99)00204-8.

[34] Del Piero G. Constitutive equation and compatibility of external loads for linear elastic masonry–like materials. Meccanica 1989;24:150–62. https://doi.org/10.1007/BF01559418.

[35] Girardi, M., Padovani, C., Pellegrini, D. Effects of the stress field on the dynamic properties of masonry bell towers. AIMETA 2017 - Proceedings of the XXIII Conference of the Italian Association of Theoretical and Applied Mechanics vol. 1 ISBN 978-889-42484-7-0.

[36] Girardi, M., Padovani, C., Pellegrini, D. Influence of temperature on the structural behaviour of masonry buildings. SAHC 2021-12th International Conference on Structural Analysis of Historical Constructions (2021), ISBN: 978-84-123222-0-0. https://doi.org/10.23967/sahc.2021.132.

[37] Teng J, Tang D-H, Hu W-H, Lu W, Feng Z-W, Ao C-F, et al. Mechanism of the effect of temperature on frequency based on long-term monitoring of an arch bridge. Struct Health Monit 2021;20(4):1716–37. https://doi.org/10.1177/1475921720931370.

[38] Giordano E, Marcheggiani L, Formisano A, Clementi F. Application of a non-invasive technique for the preservation of a fortified masonry tower. Infrastructures 2022;7:30. https://doi.org/10.3390/infrastructures7030030.

[39] Dal Cin A, Russo S. Evaluation of static and dynamic long-term structural monitoring for monumental masonry structure. J Civil Struct Health Monit 2019;9: 169–82. https://doi.org/10.1007/s13349-019-00324-z.

[40] Saisi A, Gentile C, Ruccolo A. Continuous monitoring of a challenging heritage tower in Monza. Italy J Civil Struct Health Monit 2018;8:77–90. https://doi.org/10.1007/s13349-017-0260-5.

[41] Pellegrini, D., Girardi, M., Padovani, C., Azzara, R. M. A new numerical procedure for assessing the dynamic behaviour of ancient of ancient masonry towers. M. Papadrakakis, M. Fragiadakis eds. 6th International Conference on Computational Methods in Structural Dynamics and Earthquake Engineering (COMPDYN 2017), Rodhes Island, Greece, June 15-17, 2017. https://doi.org/10.7712/120117.5783.17652.

[42] Girardi M, Padovani C, Pellegrini D. Modal analysis of masonry structures. Math Mech Solids 2019;24(3):616–36. https://doi.org/10.1177/1081286517751837.

[43] Girardi, M., Padovani, C., Pellegrini, D. and Robol, L. (2019). "Nonlinear FE model updating for masonry constructions via linear perturbation and modal analysis" in COMPDYN 2019 – 7th ECCOMAS Thematic Conference on Computational Methods in Structural Dynamics and Earthquake Engineering M. Papadrakakis, M. Fragiadakis (eds.) Crete, Greece, 24-26 June 2019. https://doi.org/10.7712/120119.6992.18689.

[44] Mottershead JE, Friswell MI. Model updating in structural dynamics: a survey. J Sound Vib 1993;167(2):347–75. https://doi.org/10.1006/jsvi.1993.1340.

[45] Ferrari R, Froio D, Rizzi E, Gentile C, Chatzi EN. Model updating of a historic concrete bridge by sensitivity-and global optimization-based Latin Hypercube Sampling. Eng Struct 2019;179:139–60. https://doi.org/10.1016/j.engstruct.2018.08.004.

[46] Bakir PG, Reynders E, De Roeck G. An improved finite element model updating method by the global optimization technique 'Coupled Local Minimizers'. Comput Struct 2008;86(11–12):1339–52. https://doi.org/10.1016/j.compstruc.2007.08.009.

[47] Mares C, Mottershead JE, Friswell MI. Stochastic model updating: part 1—theory and simulated example. Mech Syst Sig Process 2006;20(7):1674–95. https://doi.org/10.1016/j.ymssp.2005.06.006.

[48] Binante, V., Girardi, M., Padovani, C., Pasquinelli, G., Pellegrini, D., Porcelli, M., Robol, L. NOSA-ITACA 1.1 documentation (2017). www.nosaitaca.it/software/.

[49] Brincker R, Ventura C. Introduction to operational modal analysis. Wiley; 2015.

[50] Masciotta MG, Pellegrini D, Brigante D, Barontini A, Lourenço PB, Girardi M, et al. Dynamic characterization of progressively damaged segmental masonry arches with one settled support: experimental and numerical analyses. Frattura ed Integrità Strutturale 2020;14(51):423–41. https://doi.org/10.3221/IGF-ESIS.51.31.

[51] Pellegrini D, Girardi M, Lourenço PB, Masciotta MG, Mendes N, Padovani C, et al. Modal analysis of historical masonry structures: Linear perturbation and software benchmarking. Constr Build Mater 2018;189:1232–50. https://doi.org/10.1016/j.conbuildmat.2018.09.034.

[52] Pianosi F, Sarrazin F, Wagener T. A matlab toolbox for global sensitivity analysis. Environ Modell Softw 2015;70:80–5. https://doi.org/10.1016/j.envsoft.2015.04.009.

[53] Morris MD. Factorial sampling plans for preliminary computational experiments. Technometrics 1991;33(2):161–74. https://doi.org/10.2307/1269043.

[54] McKay MD, Beckman RJ, Conover WJ. Comparison of three methods for selecting values of input variables in the analysis of output from a computer code. Technometrics 1979;21(2):239–45. https://doi.org/10.2307/1268522.

[55] Brosnan DA, Sanders JP, Stroble RP. Application of thermal analysis in preservation and restoration of historic masonry materials. J Therm Anal Calorim 2013;106):109–15. https://doi.org/10.1007/s10973-013-3195-z.

[56] Dawood AO, Sangoor AJ, Al-Rkaby AHJ. Behavior of tall masonry chimneys under wind loadings using CFD technique. Case Stud Constr Mater 2020;13:e00451. https://doi.org/10.1016/j.cscm.2020.e00451.

[57] Masciotta MG, Pellegrini D. Tracking the variation of complex mode shapes for damage quantification and localization in structural systems. Mech Sys Signal Process 2022;169:108731. ISSN: 0888–3270. https://doi.org/10.1016/j.ymssp.2021.108731.

[58] Giaccone D, Santamaria U, Corradi M. An experimental study on the effect of water on historic brickwork masonry. Heritage 2020;3(1):29–46. https://doi.org/10.3390/heritage3010003.

[59] Witzany J, Cejka T, Zigler R. The effect of moisture on significant mechanical characteristics of masonry. Eng Struct Technol 2010;2(3):79–85. https://doi.org/10.3846/skt.2010.11.

[60] Wiehle P, Simon S, Baier J, Dennin L. Influence of relative humidity on the strength and stiffness of unstabilised earth blocks and earth masonry mortar. Constr Build Mater 2022;342:128026. https://doi.org/10.1016/j.conbuildmat.2022.128026.